Title
CHAPTER 3. MANY-ELECTRON AND FINAL-STATE EFFECTS: BEYOND THE ONE-ELECTRON PICTURE

Author
Shirley, David A.

Publication Date
1977-05-01

To be Published as a Chapter "Topics in Applied Physics" Photoelectron Spectroscopy of Solids

LBL-6244
Preprint
UC-34a

CHAPTER 3

MANY-ELECTRON AND FINAL-STATE EFFECTS: BEYOND THE ONE-ELECTRON PICTURE

David A. Shirley

May 1977

Prepared for the U. S. Energy Research and Development Administration under Contract W-7405-ENG-48

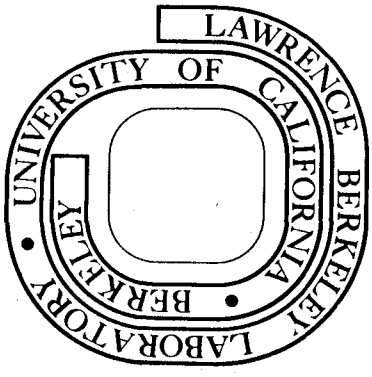

DISCLAIMER

CHAPTER 3

Many-Electron and Final-State Effects: Beyond the One-Electron Picture*

David A. Shirley

Materials and Molecular Research Division
Lawrence Berkeley Laboratory
and
Department of Chemistry
University of California
Berkeley, California 94720 U.S.A.

*This work was done with support from the U. S. Energy Research and Development Administration.

TABLE OF CONTENTS

3. Many-Electron and Final-State Effects: Beyond the One-Electron Picture.

This Chapter will serve as an introduction to the complex spectra often encountered in photoemission, when the multi-electron effects alter the spectrum. Multiplet splitting, relaxation, electron-correlation, and inelastic processes are dealt with in turn. Our goal is to delineate the physical bases of these effects. More comprehensive treatments of some related topics are given in later chapters.

3.1. Multiplet Splitting

3.1.1. Theory

To understand the effect of multiplet splitting on photoelectron spectra, let us first review the final-state structure resulting from photoemission in closed-shell systems, where multiplet structure is absent. Consider, for example, the rare-gas atom, argon. The ground-state configuration is $1s^2 2s^2 2p_{1/2}^2 2p_{3/2}^4 3s^2 3p_{1/2}^2 3p_{3/2}^4$, with level designation ^1S; i.e., $\vec{L} = \vec{S} = \vec{J} = 0$. Photoemission from any orbital, following electric dipole selection rules, leads to a ^1P final state in the N = 18 electron system. The 17-electron Ar^+ ion must, however, have the "same" quantum numbers as the orbital from which the photoelectron was ejected, with the total ^1P symmetry requirement being satisfied by coupling with the outgoing electron's continuum-wave quantum number. Thus, 1s photoemission yields a p-wave and a residual Ar^+ ion in a ^1S state. More subtly, $2p_{3/2}$ photoemission can yield an s and a d wave, but the ionic symmetry is $^2P_{3/2}$. The final-state symmetry of the ion is most readily understood by thinking of a single hole in a closed shell or subshell. For example, a single hole (like a single particle) in a $d_{5/2}$ subshell necessarily yields a state of $^2D_{5/2}$ symmetry, etc.

This result is deceptively simple. It tends to cloak the distinction between one-electron orbital quantum numbers based on a hydrogenic designation and the quantum numbers of real ionic states. This distinction is illustrated in Fig. 3.1. Because the one-hole ionic states are connected (where symmetry allows) by x-ray transitions, the implicit assumption is often made that the existence of the $K\alpha_1$, $K\alpha_2$, etc. transitions in all elements is assured and that it is somehow based on the Aufbau Principle. In fact this assumption would be wrong in two respects. First, the set of one-electron orbitals of the initial state is a somewhat arbitrary theoretical construct. No observable depends on electrons' being in these particular orbitals (e.g., Hartree-Fock orbitals) and the system could in principle be described theoretically without using them at all. Second, the final states of the unipositive ion corresponding to removal of one electron from each orbital in turn need not exist even in principle, and some do not exist in fact, as we shall see in Section 3.3. Thus certain "characteristic" x-rays are simply missing in some elements.

The above discussion has emphasized the importance of thinking in terms of final states, even for closed-shell systems. Let us now turn to multiplet splitting in open-shell systems.

The simplest case with which to illustrate the effect of multiplet splitting on photoemission is that of photoemission from a closed shell in the presence of an open shell. The simplest example is the three-electron atom typified by lithium, with a $1s^2 2s;\ ^2S$ ground state. Photoemission from the 1s orbital yields <u>two</u> final states,

$$\mathrm{Li}(1s^2 2s;\ ^2S) \rightarrow \mathrm{Li}^+(1s2s;\ ^1S) + e^-$$

$$\text{or } \mathrm{Li}^+(1s2s;\ ^3S) + e^- \quad .$$

In the Hartree-Fock approximation these states are separated in energy by $2\,G^0(1s2s)$, where $G^0(1s,2s)$ is the Slater integral for exhange in the Li^+ ion. The relative intensities of the $^3S/^1S$ lines in the photoelectron spectrum would be 3/1, the multiplet ratio. This simple example contains the essential elements of multiplet splitting in photoemission spectra.

At the next level of complexity, and the last that we shall discuss in general terms, consider photoemission from a filled s shell in the presence of an open ℓ^n shell (where $\ell^n = p^3$, d^5, etc.). VAN VLECK showed [Ref. 3.1] that the final configuration $\ell^n s$ would have two states split by

$$\Delta E = \frac{2S+1}{2\ell+1}\; G^{\ell}(s\ell) \tag{3.1}$$

in Hartree-Fock approximations, where S is the spin of the initial state. The two final states would of course have the same L value as the initial states, and their spins would be 2S and 2S+1, with the higher-spin state lying lower in energy. In this approximation the intensities would be in proportion to the multiplicity ratio; i.e., to (S+1)/S.

Multiplet splitting is also present in more complicated cases, i.e., photoemission from non-s shells. The interpretation of the spectra is straightforward but somewhat more involved. As a first step a text on multiplet coupling should be consulted [Ref. 3.2]. Often two states of the same symmetry will arise, and a simple configuration-interaction calculation is needed to obtain the eigenstates [Ref. 3.2, Appendix 21]. Fractional-parentage coefficients [Ref. 3.2, Appendix 27] are often useful for estimating intensities.

Returning to the $\ell^n s$ case, a few general comments can be made on what is to be expected in real systems, going beyond the Hartree-Fock approximation. Electron correlation will affect both the energy splitting of the multiplet and the relative peak intensities. The splitting is reduced, because even at the Hartree-

Fock level the higher-spin (lower-energy) state has less electron-electron repulsion between the s electron and the ℓ^n electrons: their parallel spins keep them apart spatially through the Pauli Principle. Electron correlation in real systems therefore lowers the energy of the lower-spin (higher-energy) state more and reduces the splitting.

The intensity ratio exceeds (S+1)/S in all known cases to date, and it appears that this result is general. Its generality is physically reasonabley, if not completely obvious. It can be attributed to loss of intensity in the lower-spin peaks, which arises through electron correlation. From the foregoing argument, the additional correlation in the low-spin state renders it less like the initial state, thereby decreasing the transition intensity by reducing the overlap of the passive orbitals. In a configuration-interaction picture this lower-spin state can admix with more configurations.

In the remainder of this section specific cases of multiplet splitting in photoemission spectra are discussed. Depth of coverage, rather than completeness, is emphasized, and no attempt is made to tabulate an exhaustive bibliography. Core and valence orbitals are treated in turn, first in 3d transition metals, then in rare earths.

3.1.2. Transition Metals

The 3d transition metal ions provide systems in which many effects characteristic of open-shell systems have been discovered and explored. An effect that is closely related to multiplet splitting in photoemission spectra is core polarization, in which a finite electron spin density, and resultant magnetic field, is created at the nucleus through "polarization" of filled inner s shells by exchange with 3d valence-electron spins. ABRAGAM and PRYCE [Ref. 3.3] explained the large hyperfine structure in $Mn^{2+}(3d^5; {}^6S)$ as arising from core

polarization of the 3s (and other) electrons by the $3d^5$ shell. They invoked a configuration-interaction picture, with 3s → 4s, etc., excitations effectively polarizing the ns^2 shells (n = 1,2,3). Interest in core polarization inspired the first study of multiplet splitting in photoemission [Ref. 3.4]. The manganous ion was chosen, because parallel coupling of the $3d^5$ electrons would be expected to enhance the effect (see Eq.(3.1)) qnd the resultant ^6S term, with $\vec{L} = 0$, should yield a simple spectrum. From Eq. (3.1), using [Ref. 3.5] $G^2(1s,3d)$ = 0.0400 eV, $G^2(2s,3d)$ = 3.512 eV, $G^2(3s,3d)$ = 10.66 eV, a maximum splitting of 12.79 eV is predicted for the 3s shell. This estimate was expected to be too high, because electron correlation should reduce ΔE, as discussed above. In fact the observed splitting in MnF_2, the most thermodynamically stable compound, is only 52% of this predicted value. In addition, the intensity ratio is about 2:1 rather than 7:5 as predicted from the ^7S:^5S final-state multiplicity ratio. In the more recent studies [Ref. 3.6] the reason for this intensity ratio was recognized as arising from electron-correlation effects, as predicted by BAGUS, et al. [Ref. 3.7]. In the configuration-interaction description of electron correlation, the ^5S final-state configuration [Ar] $3s3p^63d^5$ is admixed with configurations such as [Ar] $3s^23p^43d^6$, obtained by transferring a pair of 3p electrons to a 3s and a 3d orbital. The resulting ^5S eigenstates appear in the spectrum as the "main" ^5S peak — $^5S(1)$ in Fig. 3.2 — plus satellites, labeled $^5S(2)$ and $^5S(3)$ in Fig. 3.2. These peaks fall quite close in energy to the positions predicted by BAGUS, et al. Together with the reduction in ΔE they confirm in detail the predictions of the previous section.

Subsequent work in several laboratories has extended the observation of multiplet splitting in 3s photoelectron peaks throughout the 3d series. From the above discussion it seems clear that a correlation of ΔE with the core-polarization hyperfine field can have at best only semiquantitative significance.

Nonetheless this correlation is reasonably good [Ref. 3.8]. Figure 3.3 shows a plot of ΔE versus n for $3d^n$ ions [Ref. 3.9]. We note that the monotonic increase of $G^2(3s,3d)$ across the 3d series, together with the $(2S+1)(2\ell+1)^{-1}$ factor, can account for the variation of ΔE with n for these ions (solid curve), but that the experimental ΔE values are scaled down by a factor of two from the Van Vleck Theorem predictions. This effect of electron correlation appears to be essentially constant across the 3d series.

Multiplet splitting in the 3s peaks can also be used diagnostically, to identify the presence of localized 3d spins and hence localized moments. The first such application showed that such spins exist on iron atoms in Fe metal, [Ref. 3.4] and later this effect was shown to persist above the Curie point. [Ref. 3.10] Another interesting case is α-manganese, which is antiferromagnetic below ∿100K and paramagnetic at higher temperatures. In this case neutron scattering [Ref. 3.11] did not detect localized spins in the paramagnetic range, possibly because the interaction time is too long compared to the spin relaxation time. The speed of photoelectron spectroscopy (sampling time: 10^{-15} seconds) allows multiplet splitting to be observed on a very fast time scale, and comparison of ΔE with the ΔE vs. S correlation for manganese compounds yields [Ref. 3.12] $S = 1.2$ (and thus implies a localized magnetic moment of $1.2\mu_B$, in excellent agreement with susceptibility measurements [Ref. 3.13]). This is a clear example of photoemission as femptosecond spectroscopy.

Other s shells show the expected multiplet splitting effect in 3d metal ions. WERTHEIM, et al. [Ref. 3.14] found the 2s shells to show ΔE values close to the predictions of Eq. (3.1). This is expected because 2s and 3d electrons are already substantially radially correlated by virtue of their different principal quantum numbers, and further reduction of ΔE by configuration interaction will be slight. In the 1s shell CARLSON, et al. [Ref. 3.15] found essentially no splitting, as expected from the size of $G^2(1s,3d)$.

The filled 2p and 3p shells of the transition metal ions also show multiplet splitting. In the 3p shell of Mn^{2+} in MnF_2, the ^7P peak is easily identified, but the ^5P peak, which should, by Eq. (3.1), lie at $\sim$14 eV higher binding energy, is in fact distributed over perhaps as many as five states or more. [Refs. 3.4,3.16] This is an example of configuration interaction essentially obliterating a core-level peak. A CI calculation [Ref. 3.4] gives a good account of the observed spectrum.

In the 2p shell, multiplet effects must be present whenever the 3d electrons couple to a nonzero spin. In this case the 2p spin-orbit interaction energy is large compared to exchange energies, however, and the spectra still appear at low resolution to consist of a $2p_{1/2}$, $2p_{3/2}$ doublet. Detailed study shows more structure, however.

Again the best case appears to be manganous ion. High-resolution x-ray spectra of the $Mn(K\alpha_{12})$ lines in MnF_2 by NEFEDOV [Ref. 3.17] showed a multiple-peak character on the $K\alpha_1$ line. More recently, high-resolution x-ray photoemission studies [Ref. 3.16] confirmed this type of structure in both the $2p_{1/2}$ and the $2p_{3/2}$ peaks and revealed further peak area between these two main peaks. This work confirmed in some detail the multiplet calculations of GUPTA and SEN. [Ref. 3.18]. Although 2p-3d multiplet splitting effects are maximal (and relatively simple) in Mn^{2+}, they are expected throughout the 3d series. Evidence that they are present is obtained in the apparent increase in the spin-orbit splitting $\Delta E(2p) = E(p_{3/2}) - E(p_{1/2})$ in the 3d group. [Refs. 3.16,3.17]

In summary, multiplet splitting effects are present in Mn^{2+} in every inner shall and therefore should appear in every x-ray line.

Turning now to the valence orbitals, the final state consists of only one open shell, and its symmetry is deduced by simply removing one orbital from the

initial configuration. In the 3d group the situation is somewhat complicated by the additional presence of crystal-field effects, but it is fairly straightforward to separate the two. WERTHEIM, et al. [Ref. 3.19] noted two peaks in the 3d region of the FeF_2 valence-band spectrum. They interpreted these peaks as arising from quartet states, giving a more intense peak at higher binding energy, plus the $^6A_1$ state, giving a less intense peak at lower energy. If $Fe^{2+}(3d^6)$ is regarded as $(3d\uparrow)^5(3d\downarrow)^1$, where the arrows denote "spin up" or "spin-down", forming a quintet ground state, it is clear that removal of one 3d electron from $(3d\uparrow)^5$ can yield quartet states, while the sextet state is reached by removal of a $3d\downarrow$ electron. This interpretation is nicely reinforced by the MnF_2 valence band spectrum, in which only a single 3d peak is observed, corresponding to the quartet peak in FeF_2. The ultraviolet photoemission studies of POOLE, et al. [Ref. 3.20] show this particularly clearly, at high resolution. Of course in MnF_2 only the $(3d\uparrow)^5$ configuration is present, and only quartet final states can be formed.

3.1.3. Rare Earths

In rare-earth ions and metals the 4f electrons are quite effectively shielded from the crystal field, and atomic-structure theory can give a rather good description of multiplet effects in photoemission. Multiplet splitting of the 4s and 5s shells is particularly simple and striking. COHEN, et al. [Ref. 3.21] studied the rare-earth trifluorides, while the rare-earth metals were later studied by MC FEELY, et al. [Ref. 3.22] The 4s and 5s splittings varied little or none between the trifluorides and metals. In the 4s case, the Van Vleck relation becomes

$$\Delta E_{vv}(4s) = \frac{2S+1}{7} G^3(4s,4f) \quad .$$

As Fig. 3.4 shows, this equation correctly predicts the variation of $\Delta E(4s)$ across the rare-earth series, but the predicted magnitude is too large. A scaled-down curve, given by

$$\Delta E = 0.55\ \Delta E_{vv}$$

gives a better, though still not perfect, fit to the data. This scale factor is close to the factor of 1/2 found in the 3d series, and is believed to arise for the same reason. With principal quantum numbers the same, the 4s and 4f electron-orbitals have similar radii and therefore experience substantial correlation, which reduces the multiplet splitting.

A very nice corroboration of this interpretation is provided by the 5s shell splitting. In this case a good deal of "radial correlation" — or more accurately, radial separation — is provided by the different radii of 4f and 5s orbitals. The Van Vleck relation

$$\Delta E_{vv}(5s) = \frac{2S+1}{7}\ G^3(4f,5s) \qquad (3.2)$$

in fact predicts the observed splittings quite accurately (Fig. 3.4), with no reduction factor.

Non-s core levels couple to the $4f^n$ configurations in more complex ways, but multiplet splitting effects are often apparent. An early study [Ref. 3.10] first showed an anomalous 4d photoelectron spectrum from gaseous Eu, with an anomalous "$4d_{5/2}/4d_{3/2}$" intensity ratio of 2.5. With the advent of higher-resolution spectrometers, the Eu^{2+} 4d spectrum could be partially resolved into its multiplet components. These are most readily understood in intermediate coupling. The relevant shells are $4d^{10}(^1S)4f^7(^8S);\ ^8S$ in the initial state and $4d^9(^2D)4f^7(^8S);\ ^7D$ or ^9D (in L-S coupling notation). Using a theoretical approach developed by JUDD [Ref. 3.23] for the optical levels of the configuration $4f^7(^8S)5d^1$, KOWALCZYK, et al. [Ref. 3.24] were able to identify and assign all five components (J = 2-6)

of the ^9D term of $Eu^{3+}(4d^9 4f^7)$ in Eu metal. This is the "$4d_{5/2}$" peak — a notation that would in fact be correct only in strong j-J coupling. The ^7D peak (not $4d_{3/2}$) was unresolved: it was interpreted as being both compressed and reduced in magnitude by configuration interaction, similar to the ^5S peak in Mn^{3+} ($3s^1 3s^5$). Recently, POLLAK [Ref. 3.25] has obtained a very clean spectrum of the Eu 4d region in EuTe, reproduced in Fig. 3.5.

As a final example of multiplet splitting in rare-earth core-level spectra, we consider mixed-valence states of certain rare-earth elements. This topic has been extensively studied by groups at Bell Laboratories and IBM. [Ref. 3.26] It will be treated in detail in Chapter 8. In this section we shall simply review briefly the example of the 4d spectra of Sm^{2+}/Sm^{3+}, to establish the connection with multiplet splitting and show the diagnostic power of multiplet splitting in another application.

Divalent Sm^{2+} has the configuration $4f^6$, while Sm^{3+} is $4f^5$. The $4f^6$ configuration couples to ^7F in the free ion, with $^7F_0$ as the lowest level, according to Hund's rules. Multiplet structure through coupling to inner-shell holes in photoemission final states is small: it would of course be zero in the limit of a pure $^7F_0$ state. By contrast, the $4f^5$ configuration couples to ^6H, with $^6H_{5/2}$ lowest. Multiplet coupling with a 4d hole can yield a complicated characteristic pattern. Because of the large shift in rare-earth core-level binding energies from $4f^n$ to $4f^{n-1}$, [Ref. 3.27] the 4d spectra from these two states are well-separated. Their relative intensities yield the Sm^{2+}/Sm^{3+} ratio in mixed-valence compounds. The two above-mentioned groups have used this technique to identify mixed valence in a number of cases. Figure 3.6 shows a 4d spectrum of Sm metal from the thesis of S. P. KOWALCZYK. [Ref. 3.28] Comparison with the Sm 4d spectra given by CHAZAVIEL, et al. [Ref. 3.29] for Sm^{2+} in SmTe and Sm^{3+} in SmSb shows that Sm metal is indeed in a mixed-valence state. By contrast, the Sm 4d spectrum

of $SmA\ell_2$ shows only the 3+ lines, indicating that in this intermetallic compound samarium is essentially trivalent. Clearly core-level multiplet structure has diagnostic value for determining valence states of rare-earth alloys.

Rare-earth valence shells give the ultimate examples of multiplet splitting. The first identification and interpretation of the 4f electron structure in photoemission from rare earths was reported by HAGSTRÖM and co-workers. [Refs. 3.30, 3.32] Subsequent refinements — notably higher resolution — have yielded very detailed valence-band spectra of the rare-earths. [Ref. 3.33] A detailed treatment will be given in Chapter 8. We note here only that the photoemission spectrum of a rare earth of configuration $4f^n$ is closely related to the optical levels of the $4f^{n-1}$ configuration. In fact the spectrum can contain those multiplet components that are reached by removing one 4f electron from the $4f^n\ {}^{2S+1}L_j$ ground initial state. In most rare earths this yields a complicated multiplet structure.

3.2 Relaxation

Photoemission from an N-electron system leads to a manifold of states of the N-electron system in which one electron is unbound. Each of these states can be described in the limit of infinite separation as an (N-1)-electron state and a single free electron of kinetic energy

$$K = h\nu - E_f^{N-1} + E_i^N \quad .$$

Here $h\nu$ is the photon's energy, E_i^N is the energy of the initial state and E_f^{N-1} that of the (N-1)-electron final state. The binding energy of the orbital from which this electron was ejected is defined as

$$E_B \equiv E_f^{N-1} - E_i^N \quad . \tag{3.3}$$

In this description, which is completely rigorous, and can be closely related to empirical quantities, there is no need for the concept of a relaxation energy.

No detailed description is given of the initial or final state, and we do not allude to one-electron orbitals, let alone their separability.

Electronic structure theories are usually developed in terms of one-electron orbitals, with the coordinates of the electron coupled through self-consistent field formulations (e.g., the Hartree-Fock method). These orbitals can be described quite effectively in terms of a basis set with quantum-number designations 1s, 2s, $2p_{1/2}$, $2p_{3/2}$, etc. If multiplet splitting is neglected (e.g., for closed-shell systems; see Sect. 3.1 above), these orbital designations also label the photoelectron peaks. Moreover, solving the Hartree-Fock equations, which are sometimes termed "pseudo-eigenvalue" equations, yields a set of parameters ε_j termed "orbital energies". KOOPMANS showed [Ref. 3.34] that these orbital energies would be the binding energies $E_B(j)$ if (a) there were no change in the other orbitals when an electron was removed from orbital j, and (b) if the Hartree-Fock method gave a true description of the system. In fact for most situations encountered in photoemission the approximation

$$-\varepsilon_j \approx E_B(j) \tag{3.4}$$

is close enough for diagnostic purposes. It has become customary to write

$$E_B(j) = -\varepsilon_j - E_R(j) - \Delta E_{corr} - \Delta E_{rel} \tag{3.5}$$

or, less accurately,

$$E_B(j) \cong -\varepsilon_j - E_R(j) \quad . \tag{3.6}$$

Equation (3.5) defines the "relaxation energy" $E_R(j)$, as well as corrections for differential correlation and relativistic energies, which are of course not included in the Hartree-Fock approximation. Both of these latter effects are often neglected because they are usually small. Equation (3.2) serves as an approximate

working definition of the relaxation energy as just the reduction of the binding energy from the orbital energy. Because in periodic lattices the theoretical treatment is rarely as accurate as Hartree-Fock quality, [Ref. 3.35] this approximation will be used below.

3.2.1. The Energy Sum Rule

It is important, before discussing relaxation energies per se, to understand the relation of E_R to other features of a photoemission spectrum. A detailed discussion of this subject would entail a substantial excursion into many-body theory, which is beyond the scope of this Chapter. A recent review by GADZUK [Ref. 3.36] gives a thorough discussion of many-body effects in photoemission from a theoretical viewpoint. We shall be content with noting that the photoemission spectrum of a core level in a solid does not consist simply of one peak, but rather of a complex excitation spectrum, of which the peak is the most obvious — and lowest binding-energy — feature. Satellite structure is in principle always present due to the creation of phonons, electron-hole pairs and intrinsic plasmons during photoexcitation. [Ref. 3.36] The details of this structure will vary in a way that is hard to predict and is still far from settled experimentally even for simple materials. However, the spectral function for a core hole state, [Ref. 3.37] $N_+(\varepsilon-\omega)$, is related to the Hartree-Fock orbital energy ε_0 by a sum rule due to B. LUNDQVIST: [Ref. 3.38]

$$\int_{-\infty}^{\infty} N_+(\varepsilon-\omega)\ \varepsilon d\varepsilon = \varepsilon_0 \quad . \tag{3.7}$$

This relation is valid only in the sudden-approximation limit, so it is of little direct use in interpreting spectra (it would be impractical, for example, to evaluate ε_0 as the center of gravity of an experimental spectrum). As a conceptual tool, however, Eq. (3.7) is useful in showing the relation between the relaxation energy (i.e., the separation of the main peak from ε_0) and the satellite

structure. When one of these quantities is large, the other must be correspondingly large. Hence E_R is manifestly a many-body parameter, and any theoretical model that treats it otherwise can only be approximate. GADZUK has reviewed the various rigorous many-body approaches to this problem. We now turn to a very approximate model, and seek to understand the E_R term in solids by building up from atomic parameters.

3.2.2. Relaxation Energies

Let us first discuss atomic relaxation under its various constituent parts. Then extra-atomic relaxation will be considered for ionic and covalent materials, and for metals.

3.2.2.1. Atomic Relaxation

Removal of an electron from a given atomic shell, of principal quantum number n, creates a hole of (relative) positive charge toward which the remaining one-electron orbitals can relax. They do so adiabatically, imparting additional energy to the outgoing electron; i.e., lowering its binding energy. HEDIN and JOHANSSON [Ref. 3.39] considered the effect of relaxation of the "passive" orbitals on the total binding energy of orbital i. They partitioned the relaxation energy of orbital i into three terms,

$$E_R(i,n) = E_R(n'<n) + E_R(n'=n) + E_R(n'>n) \quad , \tag{3.8}$$

arising from the relaxation of occupied orbitals with principal quantum number n'. For each term the relaxation energy was shown to be given by a polarization potential $V_i^*-V_i$, where V_i and V_i^* are the potential at the active orbital before and after relaxation of the occupied orbitals, respectively. In this dynamical relaxation process, they showed that a factor of 1/2 arises because the relaxation occurs simultaneously with electron emission,

$$E_R(i,n) \cong \frac{1}{2} \langle n|(V^*-V)|n \rangle \quad . \tag{3.9}$$

This result is very general.

The first term in Eq. (3.4), $E_R(n'<n)$, arises from inner-shell relaxation. It is always small, for an obvious physical reason: its classical equivalent is the response of a charge distribution inside a hollow spherical conductor to a variation in charge on the spherical shell. Since V is constant inside, irrespective of this charge, there is no effect classically. In an atom, the 1s electrons' charge distribution is little affected by ionization in outer shells, etc. Thus $E_R(n'<n)$ is usually less than 1 eV and can often be safely neglected.

The $E_R(n'=n)$ term for intra-shell relaxation is larger. It is also more difficult to explain with a simple picture. A classical analogy would be obtained by distributing point charges on a spherical shell to minimize their mutual repulsion energy, then removing one charge and allowing the rest to redistribute. This picture is extremely crude, but can be useful in making a rough estimate of $E_R(n'=n)$. [Ref. 3.40] A better physical insight is obtained by thinking of the electrons in the shell as being in orbits that are optimal for the self-consistent field set up both by themselves and by the ion core. When the former is reduced in magnitude, the total potential changes and the wavefunctions relax accordingly. Calculated intra-shell relaxation energies are typically 1-3 eV in magnitude.

The "outer-shell" relaxation energy, $E_R(n'>n)$ is at once the most important and the easiest to understand and estimate using simple models. An electron in shell n will almost completely shield an orbital with $n'>n$ from one unit of nuclear charge. "Equivalent core" models for atoms, based on this principle, have been in use since the 1920's. In the case at hand, it has been shown [Ref. 3.41] that $E_R(i,n)$ values for core electrons can be estimated with surprising accuracy by considering only $E_R(n'>n)$ and using the polarization-potential model of HEDIN

and JOHANSSON together with an equivalent-cores approach based on the Slater integrals. Thus for example the 2s, $2p_{1/2}$, and $2p_{3/2}$ orbitals were estimated to have E_R values of 32 eV each, leading to binding energies of 1926, 1730, and 1676 eV, respectively. The experimental values are 1924.6, 1730.9, and 1678.4 eV. Although this agreement arises in part from systematic cancellation of errors, it is clear that $E_R(n'>n)$ estimates based on this model are quite accurate. A number of self-consistent field calculations of $E_R(i,n)$ are now available. In addition to the work of HEDIN and JOHANSSON, the original "ΔSCF" calculation of BAGUS should be mentioned, [Ref. 3.42] as well as the compilation for $Z \leqslant 29$ by GELIUS. [Ref. 3.43]

3.2.2.2. Extra-Atomic Relaxation

In addition to atomic relaxation, which is present in free atoms or condensed phases, additional contributions to the relaxation energy can always be expected in condensed phases. This additional term is often called extra-atomic relaxation. It arises because the sudden creation of a positive charge in a medium tends to polarize the medium's electronic charge toward the positive hole. The Born-Oppenheimer approximation is valid for photoemission well above threshhold; that is, the electronic charge distribution can respond at optical frequencies and can therefore, through the dynamical polarization term, make essentially the entire relaxation energy felt in the binding energy of the outgoing electron, [Ref. 3.44] which leaves on a time scale of 10^{-15} sec. The atomic nuclei are effectively frozen in place during this process, as they respond in approximately a vibrational period; i.e., 10^{-13} sec. or longer.

The extra-atomic relaxation energy accompanying photoemission from orbital i can be regarded as simply additive to the atomic term,

$$E_R(i) = E_R^a(i) + E_R^{ea}(i) \quad . \tag{3.10}$$

Of course there is no unique way to split $E_R(i)$ up into these two terms, but Eq. (3.10) is a useful approximate relation. While the general concept of extra-atomic relaxation is clear, the detailed mechanisms for its implementation (or at least our descriptions of these mechanisms) differ from ionic to covalent to metallic materials, which are therefore treated separately below.

On creation of an electronic hole state in an ionic solid, extra-atomic relaxation cannot easily take place via (fast) electronic relaxation. There are no covalent bands or itinerant electron states, through which electronic charge could be readily transferred. The available mechanisms for screening the incremental positive charge are relaxation of neighboring ions and polarization of the electronic charge on those ions. The former is too slow to affect the active electron's binding energy, so only the latter is effective.

FADLEY, et al. [Ref. 3.45] first considered the effect of the electronic polarization energy on core-level binding energies in an ionic lattice, using a model due to MOTT and GURNEY. [Ref. 3.46] They concluded that the lattice contribution to the relaxation energy is typically 1 eV or less in several potassium salts. CITRIN and THOMAS [Ref. 3.47] used a similar analysis for a series of alkali halides, in which the polarization energy should be maximal. They added a repulsion term, obtaining for the binding energy

$$E_B(i) = E_B(i,FI) + \phi\frac{e^2}{R} - E(i,REP) - E_R(i,latt) \quad . \qquad (3.11)$$

Here $E_B(i,FI)$ is the binding energy of orbital i in the free ion, $\phi e^2/R$ is the usual Madeling term, and $E_R(i,latt)$ is the extra-atomic relaxation energy for this case. These authors used a method given by MOTT and LITTLETON [Ref. 3.48] to estimate upper limits for $E_R(i,latt)$ between 1.45 eV and 2.69 eV for eleven alkali halides. By including this term they were able to improve the differences between calculated and measured core level binding energies in cations and anions. Thus

the extra-atomic term for alkali halides appears to be about 2 eV. Supporting evidence for this value is obtained from an analysis of Auger relaxation energies by KOWALCZYK, et al. [Ref. 3.49] These workers found values around 4 eV for the Auger term, which they showed should be about twice the size of the $E_R(i,latt)$ term for photoemission.

In lattices of non-monatomic ions the lattice contribution to E_R^{ea} will be smaller than for monatomic ionic lattices, because charge separation is greater. However, considerable relaxation can occur through bonds within complex ions (see below).

Extra-atomic relaxation can take place effectively through chemical bonds in molecules. Presumably this is also true for molecular solids, covalently-bonded semiconductors and semimetals, and within complex ions. Of all these cases, only free molecules are quantitatively understood, but it is probably safe to generalize for the other cases.

In free molecules, extra-atomic relaxation can be studied quite rigorously, because self-consistent molecular orbital calculations may be readily performed at several levels of sophistication. It is instructive to consider three types of orbitals separately.

Core levels are manifestly localized, and creation of a positive core hole on one atom can be regarded as having an effect similar to that of increasing by one unit the nuclear charge of that atom. The bonds are polarized, and electronic charge density shifts toward the active atom, screening the positive hole. Alternatively one can envision the excess positive charge as flowing outward to the outside of the molecule to minimize the added repulsive Coulomb energy. This latter picture is borne out very nicely by approximate molecular orbital calculations [Ref. 3.50] on small molecules, which yield the charges induced on ligand atoms. For example, in methane or tetrafluoromethane, the positive charge

added to the molecules on C(1s) photoemission goes mostly to the outer atoms. Each hydrogen acquires an added charge of +0.26 e in CH_4, while each fluorine acquires an additional charge of +0.27 e in CF_4. This is consistent with the expectation that the positive charge will be equally divided among the four ligands in each case. In CO, an additional charge of +0.54 e is induced on the carbon atom and +0.46 e on the oxygen atom on C(1s) photoemission. The simple model would give +e/2 for each atom in a diatomic molecule.

Localized molecular orbitals will behave similarly. In general E_R^{ea} will be smaller for a molecular orbital then for a core orbital, because there is no contribution analogous to outer-shell relaxation in the atomic case. Empirically it has been shown that binding-energy shifts in core orbitals and molecular orbitals localized primarily on the same atom are closely correlated for large groups of compounds. [Ref. 3.51] The E_R^{ea} term is believed to be the main contributor to both shifts in most cases.

Non-localized molecular orbitals do not show identifiable E_R^{ea} terms. First, there is no single atomic orbital to compare them with. Also, there is no particular place in the molecule for electronic charge to relax toward (i.e., no localized hole). In fact for these reasons the total relaxation energy of a nonlocalized molecular orbital will be small and may easily be outweighed by the change in correlation energy.

Extension of these ideas to semiconductors and molecular solids is rendered difficult by ambiguities in the reference energy. The core-level binding energy of one semimetal — graphite — has been predicted successfully, however. [Ref. 3.50] The approach was to calculate the E_R^{ea} term for the C(1s) orbital of the central atom in a series of small planar hydrocarbon molecules in which carbon is trigonally bonded. By extrapolating the calculated E_R^{ea} values to infinite molecular size and referring to the experimental C(1s) binding energy in benzene, a binding energy of 284.4 eV was predicted for graphite, in excellent agreement

with the experimental value of 284.7 eV.

There is no simple way to generalize this approach. A more complete understanding of relaxation energies in solids is desirable, however. This is particularly true for the valence bands of semiconductors, for which better characterization of the E_R terms would facilitate comparison of ground-state band-structure calculations with photoemission spectra.

We now consider extra-atomic relaxation in metals. Until recently it was tacitly assumed that electronic binding energies for core orbitals were unshifted in metals relative to free atoms. In fact, tables of binding energies [Ref. 3.52] were compiled by combining optical (atomic) data with x-ray (metal) data. After the importance of extra-atomic relaxation in condensed phases was appreciated, [Ref. 3.44] a careful comparison between experimental core level binding energies in metals and calculated values for free atoms showed differences

$$\Delta E_B(i) \equiv E_B(i)_{atomic} - E_B(i)_{metal} \tag{3.12}$$

ranging up to ∿15 eV. It was supposed that most of this difference arises from extra-atomic relaxation. Estimates of E_R^{ea} were made, based on the FRIEDEL model [Ref. 3.54] of alloys. In this model an added charge of +Z on an atom in a metallic lattice will be screened by its inducing positive phase shifts η_L in the partial ℓ waves of the valence-conduction band according to the Friedel Sum Rule

$$Z = \frac{2}{\pi} \sum_L (2L+1)\eta_L \quad . \tag{3.13}$$

In the present case $Z = +|e|$ and the excitonic state that is formed on photoemission will consist of a core hole shielded mostly by electronic charge drawn from states just above the Fermi energy. To obtain an upper limit on E_R^{ea}, this screening energy can be estimated by assuming the exciton to be localized on the active atom. Then E_R^{ea} can be approximated as a dynamic relaxation energy of

which the leading term is the Slater integral F^0 between the hole state and the first unfilled atomic orbital in the conduction band [Ref. 3.53]

$$E_R^{ea} \cong \left(1/2\right) F^0(i,c) \quad . \tag{3.14}$$

Using this crude model, LEY, et al. found

$$E_R^{ea}(\text{calc}) \cong 1.5\ [E_B(\text{atomic}) - E_B(\text{metal})] \tag{3.15}$$

for about 25 cases. They noted that the right-hand side also has contributions from orbital energy shifts, ΔE, but suggested that this effect is probably small. Because ab initio calculations for metals were not available, this was a moot question. Figure 3.7 illustrates the extent to which Eq. 3.15 is true, based on newer data. [Ref. 3.55]

The above approach takes specific account of the atomic structure of the active atom. An alternative approach, [Ref. 3.56] based on the dielectric properties of the substrate, gives an indication of the variation of E_R^{ea} with host material, but does not account for the specific atomic structure of the active atom. Recently WATSON, et al. [Ref. 3.57] have emphasized the importance of solid-state rehybridization and solid-state renormalization in contributing to $E_B(\text{atomic}) - E_B(\text{metal})$. They estimated the sizes of these two effects, but their calculations were (like those of LEY, et al.) open-ended, rather than being based on a self-consistent approach. Thus the relative contributions of the three effects — extra-atomic relaxation, solid-state rehybridization, and solid-state renormalization — remains an open question.

Substantial "extra-atomic" relaxation energy also accompanies ionization of an electron from the valence band in a metal. Although this fact is sometimes overlooked, it is actually implicit in the classic paper on the work function by WIGNER and BARDEEN. [Ref. 3.58] They derived an expression that can be re-arranged

to

$$E_B(\text{atomic}) + E_c - \bar{E}_B(\text{VB}) = \frac{3e^2}{5r_s} - \frac{0.458\ e^2}{r_s} \qquad (3.16)$$

where E_c is the cohesive energy, $\bar{E}_B(\text{VB})$ is the mean valence=band binding energy, and r_s is the Wigner-Seitz radius. The quantities on the right are the Coulomb and exchange energies accompanying a valence-band hole. Their sum can be construed as the extra-atomic relaxation energy. In fact the relaxation energy can be calculated as a polarization of the electron gas toward a "Coulomb hole" (for the Coulomb energy) or the "Fermi hole" (for exchange), or it can be regarded as arising from a coherent superposition of holes in valence shells on atoms, and the extra-atomic relaxation picture may be used. In either case the E_R^{ea} term amounts to several eV. [Ref. 3.59]

3.3. Electron-Correlation Effects

The correlation of electronic motion in atoms, molecules, and solids leads to the relaxation energy via Eq. (3.7), as discussed above. It also yields special structure in photoemission spectra, as alluded to for the case of Mn^{2+} in Section 3.1.2. In this Section we shall consider electron-correlation effects explicitly. Let us begin by noting a sum rule due to MANNE and ABERG: [Ref. 3.60]

$$|\epsilon| = \sum_i I_i E_B(i) \quad . \qquad (3.15)$$

This rule states that the orbital energy of a particular one-electron orbital is the centroid of all the structure in the spectrum, if the energy of each component, $E_B(i)$, is weighted by its intensity I_i. This rule is equivalent to that of LUNDQVIST, Eq. (3.7), but has a form more appropriate for atomic or molecular theory. In this Section the discussion will be couched in terms that are more familiar in molecular structure theory than in solid-state research. The reasons for this are mainly historical and because molecular theory is more advanced. It

should be noted that the results apply equally to solids. The formalism is presented first, and case studies are discussed in Section 3.3.2.

3.3.1. The Configuration Interaction Formalism

The correlation of electronic motion in a many-electron system could in principle be treated in a variety of ways. For example, the total wave functions could have as arguments various internuclear distances $\vec{r}_i - \vec{r}_j$. It is more practical, however, to work with one-electron orbitals, and this leads naturally to the method of configuration interaction, [Ref. 3.61] in which a number of configurations are admixed according to a variation principle to form each eigenstate. Thus the eigenstates of an N-electron system each have the form

$$\Psi_i(N) = \sum_j C_{ij} \Phi_j(N) \tag{3.16}$$

where $\Phi_j(N)$ is a Slater determinant of the N one-electron orbitals $\{\phi_k\}$; i.e.,

$$\Phi_j = \text{DET}\ (\phi_1^j(1),\ \phi_2^j(2),\ \ldots\ \phi_N^j(N)) \quad . \tag{3.17}$$

Here the argument of each ϕ_k refers to the electron coordinates.

Three kinds of configuration interaction (CI) are important in photoemission: final-state CI, initial-state CI, and continuum-state CI. These will be abbreviated FSCI, ISCI, and CSCI, and will be discussed separately below.

3.3.1.1. Final-State Configuration Interaction (FSCI).

This is the best-known effect. It is commonly known as "shake-up" or "shake-off" and was originally studied in rare gases by CARLSON and co-workers.[Ref. 3.62] FSCI has been oberved in many solid-state spectra as well. The effect shows up as weak satellite lines or continuum intensity associated with "primary" core-hole peaks, but at higher binding energies. In the discussion below we shall concentrate on "shake-up" because it is more important, but we note that "shake-off" can be described along similar lines.

To understand FSCI let us first approximate $\Psi_i(N)$ by its dominant configuration, which we label $\Phi_0(N)$. Next imagine photoemission from the $\ell^{\underline{th}}$ one-electron orbital. This would lead to a final state $\Phi_0'(N-1,\ell)$ in which ϕ_ℓ^0 was replaced by a continuum function χ,

$$\Phi_0'(N-1,\ell) = \text{Det}\left(\phi_1^{0'}(1),\ \phi_2^{0'}(2),\ \ldots\ \chi(\ell),\ \ldots\ \phi_N^{0'}(N)\right) \quad . \tag{3.18}$$

The matrix element for this transition would be given by terms of the form

$$\text{M.E.} \propto \langle \chi_\ell(\ell)|\vec{A}\cdot\vec{p}_\ell|\phi_\ell^0(\ell)\rangle \langle \prod_{\substack{k=1\\ \neq \ell}}^{N} \phi_k^{0'}(k) \Big| \prod_{\substack{k=1\\ \neq \ell}}^{N} \phi_k^{0}(k)\rangle \quad . \tag{3.19}$$

The first factor treats the photoelectron, shown here as electron ℓ. Of course all electrons are treated equally in the full antisymmetrized calculation. The second factor is the overlap matrix element for the passive electrons. Since $\phi_k^{0'}(k)$ and $\phi_k^0(k)$ do not overlap exactly because of relaxation, the effect of this factor is to reduce the total transition probability by typically 20-30%. Incidentally, this gives rather direct insight into the way in which relaxation (reduction in E_B) of the main line and reduction of its intensity are coupled, as indicated in Eq. (3.15).

Where does this lost intensity go? As Eq. (3.15) indicates, it must appear in satellites denoting transitions to higher-energy states in the (N-1)-electron ion. Naively these could be thought of as "shake-up" states, in each of which a passive electron was "shaken up" into a higher orbital by the sudden loss of a core electron and the accompanying sudden change in the potential. This picture had some heuristic value historically, particularly in connection with beta-decay. It is incorrect for a quantitative theory, however. One has only to note that the "shake-up" states have nothing to do with photoemission per se: they are simply eigenstates of the (N-1)-electron ion. Transitions to these states are allowed in exactly the same way as to the primary hole state. Both are N-electron transitions (or one-electron transitions if only the active electron is counted). It would be

naive — and wrong — to regard the primary and "shake-up" peaks as arising from one- and two-electron transitions, respectively.

The FSCI effect thus arises mainly from the overlap matrix element in Eq. (3.19). To isolate this effect explicity, let us suppose that the initial state is described by a single Slater determinant Φ_0, defined as in Eq. (3.17) with j = 0, and write for the final state

$$\Psi'_m(N-1,\ell) = \sum_n C_{mn}\, \Phi'_n(N-1,\ell) \tag{3.20}$$

where $\Phi'_n(N-1,\ell)$ has the form shown in Eq. (3.18). By using Eq. (3.19), with $\phi^{0'}$ generalized to $\phi^{n'}$, assuming that $\langle \chi_\ell(\ell) | \vec{A}\cdot\vec{p} | \phi^0_\ell(\ell) \rangle$ is constant for all final states, and invoking well-known properties of determinental wave functions, it can be shown [Ref. 3.63] that the intensities of transitions to all final states — primary and satellite alike — are given by

$$I(\ell,m) \propto \sum_n |C_{mn}|^2 \left| \langle \prod_{\substack{k=1 \\ \neq \ell}}^{N} \phi_k^{n'}(k) \Big| \prod_{\substack{k=1 \\ \neq \ell}}^{N} \phi_k^{0}(k) \rangle \right|^2 . \tag{3.21}$$

If the basis set $\{\phi'_k\}$ for the final state is chosen to be identical with that of the initial state (a choice that is conceptually simple but computationally inconvenient for the CI computation), then Eq. (3.21) reduces to

$$I(\ell,m) \propto |C_{m0}|^2 , \tag{3.22}$$

because $\langle \phi_k(k) | \phi_p(p) \rangle = \delta_{kp}$. We now have a complete explanation of FSCI (or "shake-up") phenomena for bound states if initial-state correlation is neglected.

3.3.1.2. Continuum-State Configuration Interaction (CSCI)

In a complete treatment of final-state configuration interaction it is often important to consider admixtures of final states in which one electron in addition to the photoelectron is unbound. [Ref. 3.64] An interesting case arises when an

excited bound state of an N-electron system lies above the ionization energy of several orbitals; i.e., if it lies in the continuum of the (N-1)-electron system. The bound state can then admix, by configuration interaction, with states formed by coupling a continuum function to an (N-1)-electron state. The resulting eigenstate, when reached by resonant photon excitation, will fall apart, leaving the (N-1)-electron states, each of which is identified by the kinetic energy of the outgoing electron. The process is referred to as "autoionization", and is well-known in atomic physics. It is not usually considered in interpreting solid-state spectra, and is usually not important because of its resonant nature. However, this process is always present when the above criteria are fulfilled, and it will not be readily separable from other CI effects.

3.3.1.3. Initial-State Configuration Interaction (ISCI).

Correlation in the final state is only half of the story. Initial-state correlation, as described by ISCI, can affect photoemission satellite spectra in two important and distinct ways. The intensities of "shake-up" lines, the positions of which are determined by final-state correlation, can be dramatically changed by initial-state correlation. In addition, new lines can appear because of ISCI, attributable to transitions that would be forbidden without this effect.

To describe the effect on intensities, let us expand the initial-state wave function $\Psi_i(N)$ to include not only its dominant component $\Phi_0(N)$ but also admixed configurations $\Phi_j(N)$ as in Eq. (3.16). We shall denote the expansion coefficients by D_{ij}. Thus

$$\Psi_0(N) = \sum_j D_{0j}\Phi_j(N) \quad . \tag{3.23}$$

The $\Phi_j(N)$ functions are of course Slater determinants of the form given in Eq. (3.17). Now the transition matrix element, Eq. (3.19), must be expanded to include sums not only over final configurations, as was done implicitly in arriving at

Eq. (3.21), but also over initial configurations. This yields a matrix element proportional to

$$\sum_{j,n} C^*_{mn} D_{0j} \langle \chi^n_\ell(\ell) | \vec{A}\cdot\vec{p}_\ell | \phi^j_\ell(\ell) \rangle \langle \prod_{\substack{k=1 \\ \neq \ell}}^{N} \phi^{n'}_k(k) | \prod_{\substack{k=1 \\ \neq \ell}}^{N} \phi^j_k(k) \rangle \tag{3.24}$$

for a transition to the $m^{\underline{th}}$ final eigenstate. If the one-electron matrix elements can be taken as approximately equal for all values of n, this expression simplifies further. We denote by $S^{\ell\ell}_{nj}$ the passive (N-1)-electron overlap matrix element which is the last factor in Eq. (3.24). With these two modifications the intensity of a given satellite including both ISCI and FSCI effects is

$$I(\ell,m) \propto \left| \sum_{j,n} C^*_{mn} D_{0j} S^{\ell\ell}_{nj} \right|^2 \tag{3.25}$$

for photoemission from the $\ell^{\underline{th}}$ orbital. The relative intensity compared to the primary peak is

$$\frac{I(\ell,m)}{I(\ell,0)} = \frac{\left| \sum_{j,n} C_{mn} D_{0j} S^{\ell\ell}_{nj} \right|^2}{\left| \sum_{j,n} C^*_{0n} D_{0j} S^{\ell\ell}_{nj} \right|^2} \quad . \tag{3.26}$$

To interpret this result physically we note that the final-state relative peak intensities are determined in this model primarily by expansion coefficients C_{mn} and D_{0j} and by overlap integrals of the <u>passive</u> electrons $S^{\ell\ell}_{nj}$. Let us focus only on the passive electrons. We also imagine that both the initial and the final state can be written as the sum of a "main" configuration (with large C_{00} and D_{00}) and a number of less important admixed configurations, with small (0.1 or less) C_{mn} and D_{0j}. Now $S^{\ell\ell}_{nj}$ is expected to be large (i.e., near unity) for n = j and small otherwise. Thus the largest contributor to the photoemission intensity arises from the $C^*_{00}D_{00}S^{\ell\ell}_{00}$ term, in the primary peak. The smaller, but dominant FSCI effect arises from the main (N-1)-electron configuration "picking itself out" as an admixed basis

state in the other final eigenstates. The relevant terms are of the form $C^*_{m0} D_{00} S^{\ell\ell}_{00}$. The intensity from this channel alone would be typically $\sim$1% of the main-line intensity. It gives a more correct description of the heuristic "shake-up" process, but cannot account for satellite intensities. Finally, the dominant FSCI channel is the mirror image of this channel. Each admixed (N-1)-electron configuration in the ground state "seeks itself out" as the dominant configuration in one of the "shake-up" states. The relevant term here in $C^*_{mm} D_{0m} S^{\ell\ell}_{mm}$. Again the intensity would be $\sim$1% for this term alone, but the satellite intensity is in fact determined from a coherent superposition of these last two channels [Ref. 3.63] (Eq. (3.25)). With this last term included, meaningful satellite intensities can be calculated.

New lines appear due to ISCI alone when final states are reached that are forbidden by dipole selection rules to be accessible from the main ground-state configuration. This situation usually arises in valence-shell photoemission.

3.3.2. Case Studies

One example of each of the above types of configuration interaction will be given briefly, for illustrative purposes. The reader is referred to the original literature for detailed discussions.

3.3.2.1. Final-State Configuration Interactions: The 4p Shell of Xe-Like Ions.

For a number of elements near xenon there are no characteristic x-rays based on transitions to or from the $4p_{1/2}$ hole state. The reason for this, as GELIUS has shown [Ref. 3.65] in a set of high-resolution photoemission experiments, is that no simple $4p_{1/2}$ hole state exists in these elements. WENDIN [Ref. 3.66] has given an elegant and complete theoretical explanation of this phenomenon in which many-body effects are shown to be explicitly involved. In the present discussion no attempt will be made to treat WENDIN'S mechanisms fully. Instead, only one of

the most important reasons for the loss of an identifiable $4p_{1/2}$ peak will be given.

Removal of a $4p_{1/2}$ electron from a xenon-like ion yields a configuration that can be written in part $[...4s^2 4p^5 4d^{10}...\varepsilon f^0]$. Here the εf state is included to mark the fact that the nearly bound continuum states must possess considerable f character as the rare-earth series is approached. In fact the above configuration can mix strongly with several others that are formed at about the same energy by a pairwise correlation that raises one 4d electron into an f orbital and drops one into a 4p orbital; i.e.,

$$[...4s^2 4p^5 4d^{10}...\varepsilon f^0] \rightarrow [...4s^2 4p^6 4d^8...nf^1] \quad .$$

Here we have substituted nf for εf to emphasize that the f orbital is bound. Several configurations can be formed by mechanisms like this because the relatively large angular momenta can couple in a variety of ways. Configuration interaction then leads to a distribution of the total transition strength among a number of eigenstates.

No single eigenstate can be identified as "the" $4p_{1/2}$ hole state. Thus in this example the simple "shake-up" picture breaks down completely. Rather than a primary peak and a number of satellites, there are instead a number of equivalent peaks.

3.3.2.2. Continuum-State Configuration Interaction: The $5p^6 6s^2$ Shell.

Continuum final states affect photoemission spectra whenever the ionization threshhold of a second electron is exceeded. The experimental manifestation of this "shake-off" phenomenon is a continuous-energy electron distribution. Of more spectroscopic interest is the resonant excitation of autoionizing states. These are states formed by admixing N(bound)-electron states embedded in the continuum with other states formed from one or more continuum electrons plus N-1 or fewer

bound electrons.

Photoionization of atomic barium provides an interesting recent example of this phenomenon. The ground-state configuration of Ba is primarily $[Xe]6s^2$. The least-bound subshell in Xe is $5p^6$. We therefore may refer to the $[...5p^6 6s^2]$ configuration as the ground state of Ba.

The binding energy of the 6s orbital is 5.211 eV: the Ba II continuum therefore starts at this energy. [Ref. 3.67] There are an infinite number of bound states of Ba II between 5.211 eV and 15.215 eV, the onset of the Ba III continuum, as shown in Fig. 3.8. The onset of ionization of the 5p shell of Ba I lies at 22.7 eV. Based on this threshhold, and at slightly lower energies, there are many Rydberg states, of the form $[...5p^5 6s^2(nd \text{ or } ns)]_{J=1}$, as evidenced by UV absorption studies. [Refs. 3.68, 3.69] Thus atomic barium is well set-up for resonant excitation of these levels by the HeI_α line (21.21 eV) or its higher-energy satellites. Resonant excitation was in fact observed, by two groups. [Refs. 3.70-3.72] It was explained by FANO, [Ref. 3.73] and has been studied further and extended to other elements by LEE, et al. [Ref. 3.67]

The barium photoemission spectrum excited by He I radiation consists of many peaks, some of which are attributable to high $n\ell$ states in Ba II, with the highest identifiable values of $n\ell$ being 10s, 10p, 9d, 7f, and 7g. [Ref. 3.67] There are also two strong triplets of low-energy peaks, falling at binding energies above the Ba III threshhold. [Ref. 3.71]

This spectrum can be explained if an excited $[...5p^5 6s^2(ns \text{ or } nd)]_{J=1}$ state of Ba absorbs the HeI_α (21.22 eV) radiation resonantly. This state mixes with continuum states based on the BaIII $[5p^6]$ ground state, on BaII $[5p^5 n\ell n'\ell']$ states and on various BaII $[5p^6 n\ell]$ states. The latter have the form BaII $[5p^6 n\ell\varepsilon\ell']$. Two types of configuration can be formed from states above the BaIII threshhold. The first involves two continuum electrons. The second consists of a discrete

BaII 5p-hole state imbedded in the BaIII continuum. The oscillator strength of the resonant transition will be shared among these continuum states. Resonant absorption and autoionization gives rise to the features observed in the photoelectron spectrum. The BaII [$5p^6 n\ell$] lines are produced directly via autoionization and detected as peaks through the kinetic energy of the continuum electron. The BaIII $5p^6$ state is formed by double autoionization of two continuum electrons from BaIII [$5p^6 \varepsilon\ell\varepsilon'\ell'$], yielding a continuous electron distribution at energies beyond the BaIII threshhold. This BaIII state may also be reached by a two-step autoionization-Auger process, yielding the two triplets reported by HOTOP and MAHR. [Ref. 3.71]

Resonant autoionization of the $5p^6$ shell by HeI radiation has been shown to occur well into the rare-earth elements. [Ref. 3.67] While sharp spectra of the type discussed here cannot be expected in solids, a broadened or continuum-like version of CSCI will often be present and must be taken into consideration.

3.3.2.3. Initial-State Configuration: Two Closed-Shell Cases.

GELIUS [Ref. 3.74] reported a high-resolution study of the x-ray photoemission spectrum of the Ne 1s core-hole region. Included in this spectrum were accurately-measured energies and intensities of several correlation-state peaks. By concentrating on the $1s2s^22p^6 \rightarrow 1s2s^22p^5np$ excitations, where n = 3,4,5, and 6, MARTIN and SHIRLEY [Ref. 3.75] were able to show that about half of the intensity in each satellite could be attributed to correlation in the ground state; i.e., ISCI. Thus configurations of the form $1s^22s^22p^5np$ were invoked for the neon ground state (as small admixtures). In fact this result implies that ground-state correlations can be studied rather directly by inspection of "shake-up" spectra, without resorting to detailed calcuation.

In photoemission from the valence shell, direct evidence for initial-state correlations has been reported [Refs. 3.67,3.76-3.78] for Groups IIA and Group IIB

atoms. In each case evidence of ISCI was provided by the observation of new lines that would not be allowed by the primary configuration. Thus, for example, the photoionization spectrum of calcium yielded peaks for the 4p, 3d, 5s, and 4d lines [Ref. 3.78] of Ca^+. This is explained by admixtures of $4p^2$, $3d^2$, etc., into the $4s^2$ ground state of Ca. Of course some of the final states may have substantial contributions from two or more initial-state configurations.

Clearly ISCI as observed by valence-shell photoemission can yield valuable and direct information about the composition of the ground state. The configuration assignments in solids are usually less clear cut. However, mixed-valence studies in rare earths (Chapter 8) provide an example of the application of ISCI in the solid state.

3.4 Inelastic Process

We finish this Chapter with a very brief discussion of inelastic effects on photoemission spectra. Electrons passing through metals lose energy in quanta, mainly through plasmon excitation. The resultant spectral features are well-known and of great interest in energy-loss spectroscopy. They are also present in photoemission spectroscopy, where they serve more to complicate the spectra than to yield new information. The discussion below is limited to the two features of plasmon losses that bear directly on photoemission spectroscopy per se: the problem of intrinsic versus extrinsic plasmon structure and the enhancement of surface sensitivity in metals.

3.4.1. Intrinsic and Extrinsic Structure

Plasmon losses in photoelectron spectroscopy are usually discussed in terms of a three-step model of photoemission, which MAHAN [Ref. 3.79] and EASTMAN and FEIBELMAN [Ref. 3.80] have shown can be derived from a Golden Rule expression.

The steps are:

(1) Optical excitation

(2) Transport to the surface, and

(3) Escape into the vacuum.

Each step can be related to a specific feature of the (primary peak and plasmon) photoemission from a core shell in a metal.

Step (1) yields the primary peak, if there is no inelastic loss arising from steps (2) and (3) as the photoelectron leaves the solid. This peak will have the maximum kinetic energy allowed,

$$K = h\nu - E_B \quad .$$

Figure 3.9 shows a valence-band and a 2p-shell spectrum of magnesium metal, taken with AlK_α x-rays.[Ref. 3.59] The peaks labeled "VB" and "2p" are the primary spectral features that contain most of the single-electron excitation information about magnesium.

Step (2), transport to the surface, yields the bulk plasmon spectrum. The peaks labeled "P1", "P2", etc., arise through excitation of 1, 2, etc. bulk plasmons as primary electrons move through the metal. These peaks are broadened by angular dispersion. Neglecting this effect, the kinetic energy of the $n^{\underline{th}}$ bulk plasmon peak lies at

$$K = h\nu - E_B - nE_p \tag{3.27}$$

where E_p is the plasmon excitation energy.

The third step affects photoelectrons in several ways (e.g., refraction). The only large effect observable in angle-integrated spectra of the types shown in Fig. 3.9 is the appearance of peaks due to surface plasmons, with a characteristic energy loss of

$$E_s = E_p/\sqrt{2} \quad .$$

The corresponding kinetic energy, for an electron that has suffered n bulk losses, then one surface loss, is

$$K = h\nu - E_B - nE_P - E_S \quad . \tag{3.28}$$

Two such peaks are identifiable in Fig. 3.9, for n = 0 and n = 1. These are labeled "P_S" and "Pl + P_S", respectively.

All of the above features are well-known from electron energy-loss spectroscopy, [Ref. 3.81] with the primary photoemission peak being equivalent to the elastic peak in energy-loss spectra. Photoemission spectroscopists must be aware of these phenomena to interpret their spectra correctly, but photoemission is not in general a particularly good method for studying loss spectra because of angular dispersion.

There are certain circumstances in which plasmon loss structure accompanying photoemission can be of unique values. Let us consider two such cases. The first involves the creation of <u>intrinsic</u> plasmons during the photoemission process — Step (1) above. Intrinsic plasmon excitation was first predicted by B. LUNDQVIST, [Ref. 3.38] and intrinsic plasmons are included as part of the spectral function $N_+(\varepsilon-\omega)$ in Eq. (3.7). Intrinsic plasmons would presumably contribute most heavily in the Pl region of the spectrum. Unfortunately it is not simple to distinguish between intrinsic and extrinsic plasmons, and the existence of intrinsic plasmons is still a subject of discussion. The difficulty is that careful intensity measurements are required to establish the existence of intrinsic plasmons, and an adequate theory is needed for the interpretation of these intensities. POLLAK, et al. [Ref. 3.82] observed bulk and surface plasmon peaks in photoemission from several clean metals. They found no strong evidence for intrinsic plasmons. Later PARDEE, et al. [Ref. 3.83] made a more detailed analysis and were again able to fit the loss spectra without the need to invoke intrinsic plasmons. These workers

found that 10% or less of the plasmon structure was required to be intrinsic by their semi-phenomenological analysis, in contrast to the theoretical expectation [Ref. 3.38] of 50% or more. It should be noted that neither this analysis nor any other semi-phenomenological approach can give a definitive answer to the question of the existence of intrinsic plasmons. A more complete theory is required: specifically one that unambiguously predicts different intensity ratios theoretically depending on whether or not intrinsic plasmons are present. Recently PENN [Ref. 3.84] has produced just such a theory and has used it to analyze the loss structure of Na, Mg, and Al, concluding that the fraction of the first loss peak due to intrinsic plasmons is 0.41, 0.36, and 0.26, respectively. Thus the intrinsic plasmon problem appears to be coming under control.

The second case in which plasmon strucutre in photoemission is of unique interest is that of surface plasmon loss accompanying photoemission from adsorbates. This effect has been little studied as yet, but it has been observed by BRADSHAW, et al. [Ref. 3.85] These workers detected Al surface plasmons on the O 1s line of oxygen adsorbed on aluminum.

3.4.2. Surface Sensitivity

Our final topic is photoemission surface sensitivity, mentioned here because it is a direct consequence of plasmon energy loss. At kinetic energies above the plasma energy, electrons traveling through metals are subject to energy loss via plasmon creation. Electrons that lose as much as even one plasmon quantum of energy (typically $\sim$10-15 eV) are effectively removed from the "full-energy" peak or structure, as in Fig. 3.9. Thus the mean attenuation length decreases markedly above the plasmon energy, and the effective sampling depth for electrons contributing to the full-energy peaks shows a very broad minimum in the electron kinetic energy range K$\sim$100 eV. Figure 3.10 shows a "Universal Curve" that represents a broad range of data on effective sampling depths in heavy metals, compiled from many

literature sources. A recent compilation has been given by BRUNDLE, [Ref. 3.86] with references to earlier work.

The Universal Curve is self-explanatory, but two comments can be made. First, the curve represents surface sensitivity for normal electron take-off angles. If electrons are accepted at lower angles, say at an angle Θ from the sample plane, then the surface sensitivity is enhanced by a factor of $(\sin\Theta)^{-1}$. In practice this can give up to a tenfold increase in the surface sensitivity; i.e., it can multiplicatively lower the effective Universal Curve by this factor (if refraction is neglected). Both the intrinsic surface sensitivity and its tunability by varying energy and angle offer great possibilities in applying photoemission to surface phenomena.

Second, the surface sensitivity in semiconductors is similar to that in metals, although as yet not nearly so well-characterized. In ordinary molecular solids the surface sensitivity appears to be much lower, presumably because the plasmon loss mechanism is absent. Molecular solids are discussed by Grobman in Chapter 9.

REFERENCES

[3.1] J. H. VAN VLECK: Phys. Rev. 45, 405 (1934)

[3.2] See, for example, J. C. SLATER: "Quantum Theory of Atomic Structure", Vol. II (McGraw-Hill), Chapters 20-22

[3.3] A. ABRAGAM and M. H. L. PRYCE: Proc. Roy. Soc. A, 205, 135 (1951)

[3.4] C. S. FADLEY, D. A. SHIRLEY, A. J. FREEMAN, P. S. BAGUS, and J. V. MALLOW: Phys. Rev. Letters 23, 1397 (1969)

[3.5] J. B. MANN: Los Alamos Scientific Laboratory Report LASL-3690 (1967). These values are for neutral atoms.

[3.6] S. P. KOWALCZYK, L. LEY, R. A. POLLAK, F. R. MCFEELY, and D. A. SHIRLEY: Phys. Rev. B7, 4009 (1973)

[3.7] P. S. BAGUS, A. J. FREEMAN, and F. SASAKI: Phys. Rev. Letters 30, 850 (1973)

[3.8] S. HÜFNER and G. K. WERTHEIM: Phys. Rev. B7, 2333 (1973)

[3.9] D. A. SHIRLEY: Physica Scripta 11, 117 (1975)

[3.10] C. S. FADLEY and D. A. SHIRLEY: Phys. Rev. A2, 1109 (1970)

[3.11] C. G. SHULL and M. K. WILKINSON: Rev. Mod. Phys. 23, 100 (1953)

[3.12] F. R. MCFEELY, S. P. KOWALCZYK, L. LEY, and D. A. SHIRLEY: Solid State Commun. 15, 1051 (1974)

[3.13] H. NAGASAWA and M. UCHINAMI: Phys. Letters 42A, 463 (1973)

[3.14] Reference 3.8, Fig. 1. Also see Ref. 3.6.

[3.15] T. A. CARLSON, J. C. CARVER, and G. A. VERNON, J. Chem. Phys. 62, 932 (1975)

[3.16] S. P. KOWALCZYK, L. LEY, F. R. MCFEELY, and D. A. SHIRLEY: Phys. Rev. B11, 1721 (1975)

[3.17] V. I. NEFEDOV: Dokl. Akad. Nauk Ser. Fiz. 28, 816 (1964) [Bull. Acad. Sci. U.S.S.R. Phys. Ser. 28, 724 (1964)]

[3.18] R. P. GUPTA and S. K. SEN: Phys. Rev. B10, 71 (1974)

[3.19] G. K. WERTHEIM, H. J. GUGGENHEIM, and S. HÜFNER: Phys. Rev. Letters 30, 1050 (1973)

[3.20] R. T. POOLE, J. D. RILEY, J. G. JENKIN, J. LIESEGANG, and R. C. G. LECKEY: Phys. Rev. B13, 2620 (1976)

[3.21] R. L. COHEN, G. K. WERTHEIM, A. ROSENCWAIG, and H. J. GUGGENHEIM: Phys. Rev. B5, 1037 (1972)

[3.22] F. R. MCFEELY, S. P. KOWALCZYK, L. LEY, and D. A. SHIRLEY: Phys. Letters 49A, 301 (1974)

[3.23] B. R. JUDD: Phys. Rev. 125, 613 (1962)

[3.24] S. P. KOWALCZYK, N. EDELSTEIN, F. R. MCFEELY, L. LEY, and D. A. SHIRLEY: Chem. Phys. Letters 29, 491 (1974)

[3.25] R. A. POLLAK: private communication, December, 1976

[3.26] For early work, see M. CAMPAGNA, E. BUCHER, G. K. WERTHEIM, D. N. E. BUCHANAN, and L. D. LONGINETTI: Phys. Rev. Letters 32, 885 (1974), and R. A. POLLAK, F. HOLTZBERG, J. L. FREEOUF, and D. E. EASTMAN: Phys. Rev. Letters 33, 820 (1974). Later references are given in Chapter 8.

[3.27] C. S. FADLEY, S. B. M. HAGSTRÖM, J. M. HOLLANDER, M. P. KLEIN, and D. A. SHIRLEY: Science 157, 1571 (1967)

[3.28] S. P. KOWALCZYK: Ph.D Thesis, University of California, 1976. Lawrence Berkeley Laboratory Report LBL-4319

[3.29] J.-N. CHAZALVIEL, M. CAMPAGNA, G. K. WERTHEIM, and P. H. SCHMIDT: Phys. Rev. B14, 4586 (1976)

[3.30] G. BRODÉN, S. B. M. HAGSTRÖM, P.-O. HEDÉN, and C. NORRIS: Proc. 3rd IMR Symposium Nat. Bur. Stand. Spec. Publ. 323 (1970)

[3.31] P.-O. HEDÉN, H. LÖFGREN, and S. B. M. HAGSTRÖM: Phys. Rev. Letters 26, 432 (1971)

[3.32] G. BRODÉN, S. B. M. HAGSTRÖM, and C NORRIS: Phys. Rev. Letters 24, 1173 (1971)

[3.33] Y. BAER, and G. BUSCH, in: "Electron Spectroscopy. Progress in Research and Application", ed. by R. CANDANO and J. VERBIST (Elsevier, 1974) p. 611.

[3.34] T. KOOPMANS: Physica 1, 104 (1934)

[3.35] But see J. G. GAY, J. R. SMITH, and F. J. ARLINGHAUS: Phys. Rev. Letters 38, 561 (1977) for a self-consistent calculation in copper.

[3.36] J. W. GADZUK: "Many-Body Effects in Photoemission", Chaper 7 in "Photoemission from Surfaces", ed. by B. FEUERBACHER, B. FITTON, and R. F. WILLIS (John Wiley and Sons)

[3.37] $N_+(\varepsilon-\omega)$ is the imaginary part of the hole Green's function (see Ref. [3.36]). It has units of $(\text{energy})^{-1}$.

[3.38] B. LUNDQVIST: Phys. Kondens. Mater. 6, 193 (1967); 6, 206 (1967); 7, 117 (1968); 9, 236 (1969)

[3.39] L. HEDIN and A. JOHANSSON: J. Phys. B 2, 1336 (1969)

[3.40] R. L. MARTIN and D. A. SHIRLEY: "Many-Electron Theory of Photoemission", Chapter to be published in "Electron Spectroscopy: Theory, Techniques, and Applications", A. D. BAKER and C. R. BRUNDLE, editors (Academic Press)

[3.41] D. A. SHIRLEY: Chem. Phys. Letters 16, 220 (1972)

[3.42] P. S. BAGUS: Phys. Rev. 139, A619 (1965)

[3.43] U. GELIUS: Physica Scripta 9, 133 (1974)

[3.44] But see Chapter 4 for a careful discussion of the extent to which this is true.

[3.45] C. S. FADLEY, S. B. M. HAGSTROM, M. P. KLEIN, and D. A. SHIRLEY: J. Chem. Phys. 48, 3779 (1968)

[3.46] N. F. MOTT and R. W. GURNEY: Electronic Processes in Ionic Crystals, Clarendon Press, Oxford, 1948 (2nd Edition)

[3.47] P. A. CITRIN and T. D. THOMAS: J. Chem. Phys. 57, 4446 (1972)

[3.48] N. F. MOTT and N. J. LITTLETON: Trans. Faraday Soc. 34, 485 (1938)

[3.49] S. P. KOWALCZYK, L. LEY, F. R. MCFEELY, R. A. POLLAK, and D. A. SHIRLEY: Phys. Rev. B8, 2392 (1973)

[3.50] D. W. DAVIS and D. A. SHIRLEY: J. Electr. Spectr. and Rel. Phen. 3, 137 (1974)

[3.51] B. E. MILLS, R. L. MARTIN, and D. A. SHIRLEY: J. Amer. Chem. Soc. 98, 2380 (1976)

[3.52] J. A. BEARDEN and A. F. BURR: Rev. Mod. Phys. 31, 616 (1967)

[3.53] L. LEY, S. P. KOWALCZYK, F. R. MCFEELY, R. A. POLLAK, and D. A. SHIRLEY: Phys. Rev. B8, 2392 (1973)

[3.54] J. FRIEDEL: Philos. Mag. 43, 153 (1952); Adv. Phys. 3, 445 (1954)

[3.55] D. A. SHIRLEY, R. L. MARTIN, S. P. KOWALCZYK, F. R. MCFEELY, and L. LEY: Phys. Rev. B15, 544 (1977)

[3.56] P. H. CITRIN and D. R. HAMANN: Chem. Phys. Letters 22, 301 (1973)

[3.57] R. E. WATSON, M. L. PERLMAN, and J. F. HERBST: Phys. Rev. B13, 2358 (1976)

[3.58] E. WIGNER and J. BARDEEN: Phys. Rev. 48, 84 (1935)

[3.59] L. LEY, F. R. MCFEELY, S. P. KOWALCZYK, J. G. JENKIN, and D. A. SHIRLEY: Phys. Rev. B11, 600 (1975)

[3.60] R. MANNE and T. ABERG: Chem. Phys. Letters 7, 282 (1970).

[3.61] See Chapter 5, by S. T. MANSON, and references therein for a discussion of configuration interaction.

[3.62] T. A. CARLSON: Phys. Rev. 156, 142 (1967): D. P. SPEARS, J. H. FISCHBECK, and T. A. CARLSON: Phys. Rev. A9, 1603 (1974) and references therein.

[3.63] R. L. MARTIN and D. A. SHIRLEY: J. Chem. Phys. 64, 3685 (1976).

[3.64] U. FANO and J. W. COOPER: Rev. Mod. Phys. 40, 441 (1968).

[3.65] U. GELIUS: J. Elect. Spectr. and Rel. Phen. 5, 985 (1974).

[3.66] S. LUNDQVIST and G. WENDIN: J. Elect. Spectr. and Rel. Phen. 5, 513 (1974)

[3.67] S.-T. LEE, Ş. SÜZER, E. MATTHIAS, R. A. ROSENBERG, and D. A. SHIRLEY: J. Chem. Phys. 66, 2496 (1977)

[3.68] J. P. CONNERADE, M. W. D. MANSFIELD, K. THIMM, and D. TRACY: VUV Radiation Physics, ed. by E. E. KOCH, R. HAENSEL, and C. KUNZ (Pergamon, Vieweg, 1974), p. 243

[3.69] D. L. EDERER, T. B. LUCATORTO, and E. B. SALOMON: VUV Radiation Physics, ed. by E. E. KOCH, R. HAENSEL, and C. KUNZ (Pergamon, Vieweg, 1974), p. 245

[3.70] B. BREHM and K. HÖFLER: Int. J. Mass Spectrom. Ion Phys. 17, 371 (1975)

[3.71] H. HOTOP and D. MAHR: J. Phys. B8, L301 (1975)

[3.72] U. FANO: Comments on At. and Mol. Phys. 4, 119 (1973)

[3.73] J. E. HANSEN: J. Phys. B8, L403 (1975)

[3.74] U. GELIUS: J. Electr. Spectr. and Rel. Phen. 5, 985 (1974)

[3.75] R. L. MARTIN and D. A. SHIRLEY: Phys. Rev. A13, 1475 (1976)

[3.76] Ş. SÜZER and D. A. SHIRLEY: J. Chem. Phys. 61, 2481 (1974)

[3.77] J. BERKOWITZ, J. L. DEHMER, Y. K. KIM, and J. P. DESCLAUX: J. Chem. Phys. 61, 2556 (1974)

[3.78] Ş. SÜZER, S.-T. LEE, and D. A. SHIRLEY: Phys. Rev. 13, 1842 (1976)

[3.79] G. D. MAHAN: Phys. Rev. B2, 4334 (1970)

[3.80] F. J. FEIBELMAN and D. E. EASTMAN: Phys. Rev. B10, 4932 (1974)

[3.81] H. RAETHER: Springer Tracts in Modern Physics 38, 84 (1965)

[3.82] R. A. POLLAK, L. LEY, F. R. MCFEELY, S. P. KOWALCZYK, and D. A. SHIRLEY: J. Electr. Spectr. and Rel. Phen. 3, 381 (1974)

[3.83] W. J. PARDEE, G. D. MAHAN, D. E. EASTMAN, R. A. POLLAK, L. LEY, F. R. MCFEELY, S. P. KOWALCZYK, and D. A. SHIRLEY: Phys. Rev. B11, 3614 (1975)

[3.84] DAVID R. PENN: private communication.

[3.85] A. M. BRADSHAW, W. DOMCKE, and L. S. CEDARBAUM: Phys. Rev. B15, XXXX (1977)

[3.86] C. R. BRUNDLE: Surface Science 48, 99 (1975)

FIGURE CAPTIONS

Figure 3.1 Illustration of the one-electron orbital picture (left) and the true energy-level diagram of neon. The orbital energies ε are not observables and do not give exact binding energies or x-ray transition energies, while true energy levels do. Note that the ^1S(Ne) ground state is a state of atomic neon, while other states are in Ne^+.

Figure 3.2 Multiplet structure in the Mn 3s shell, in AlK_α x-ray photoemission from MnF_2, after Reference 3.6.

Figure 3.3 The 3s multiplet splitting in 3d metal oxides and fluorides (circles), and predictions based on Van Vleck's Theorem (line). Note scale reduction factor of two between theory and experiment. After Reference 3.9.

Figure 3.4 Experimental 4s and 5s splitting in rare-earth fluorides (open circles) and metals (filled circles), and the theoretical values based on Van Vleck's Theorem (lines). Note reduction factor for 4s case but not for 5s. After References 3.21 and 3.22.

Figure 3.5 The Eu 4d photoelectron spectrum of EuTe, taken by R. A. POLLAK of IBM Laboratories, using AlK_α radiation, with a sample temperature of 50K. The left peak is the ^7D manifold, and the ^9D manifold is resolved into components in the right peak.

Figure 3.6 The Sm 4d region of samarium metal, showing the AlK_α x-ray photoemission spectrum of a clean speciman under ultra-high vacuum conditions. Most of this spectrum is from Sm^{3+}. The peak at 124 eV arises from Sm^{2+}, and proves that Sm is in a mixed-valence state in samarium metal. After Reference 3.28.

Figure 3.7 Difference between core-electron (mostly 2p) binding energies in free atoms and metals for several elements, plotted against extra-atomic relaxation energy as estimated from Eq. (3.15). Most of the E_B (atomic) values used were theoretical.

Figure 3.8 Energy levels in BaI (atomic Ba), BaII, and BaIII, illustraing autoionization by the HeI_α line, but not by NeI radiation. After Reference 3.67. The $5p^5 6s5d$ level in BaII is an intermediate in a two-step process discovered by HOTOP and MAHR [Ref. 3.71].

Figure 3.9 Photoelectron spectra of valence-band region (top) and 2p region (bottom) of magnesium metal, taken with AlK_α radiation. Note plasmon loss structure.

Figure 3.10 The Universal Curve of electron attenuation length in various heavy metals, drawn as a band that encompasses most of the existing experimental data (see [Ref. 3.36]). The energies of several laboratory photon sources are shown for reference.

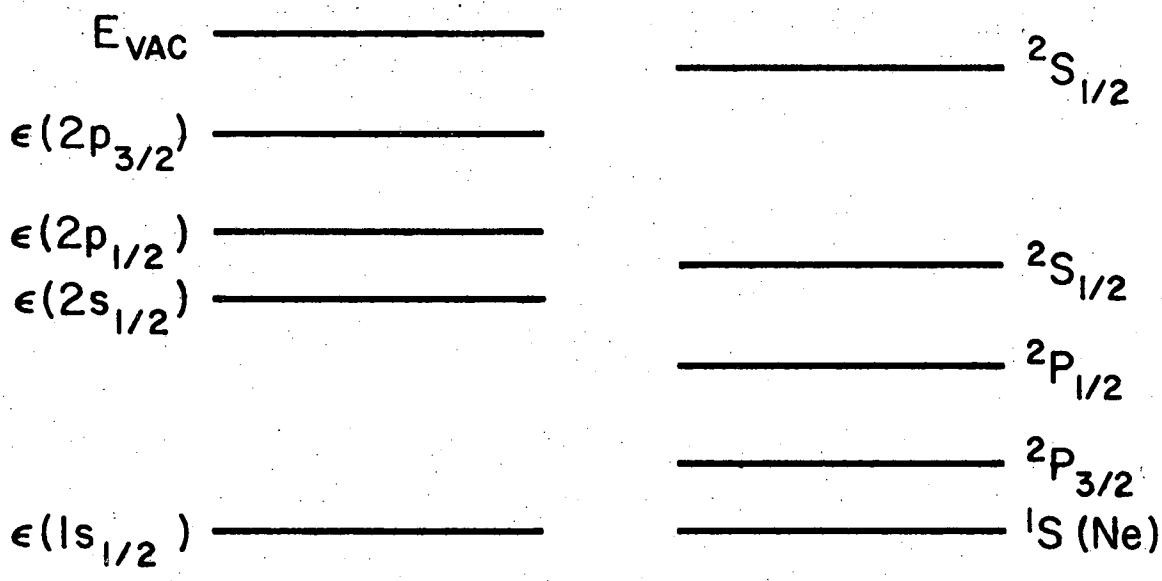
E_{VAC}
$\epsilon(2p_{3/2})$
$\epsilon(2p_{1/2})$
$\epsilon(2s_{1/2})$
$\epsilon(1s_{1/2})$
$^2S_{1/2}$
$^2S_{1/2}$
$^2P_{1/2}$
$^2P_{3/2}$
^1S (Ne)
ORBITAL ENERGIES
ENERGY LEVELS
XBL 774-906

Fig. 1

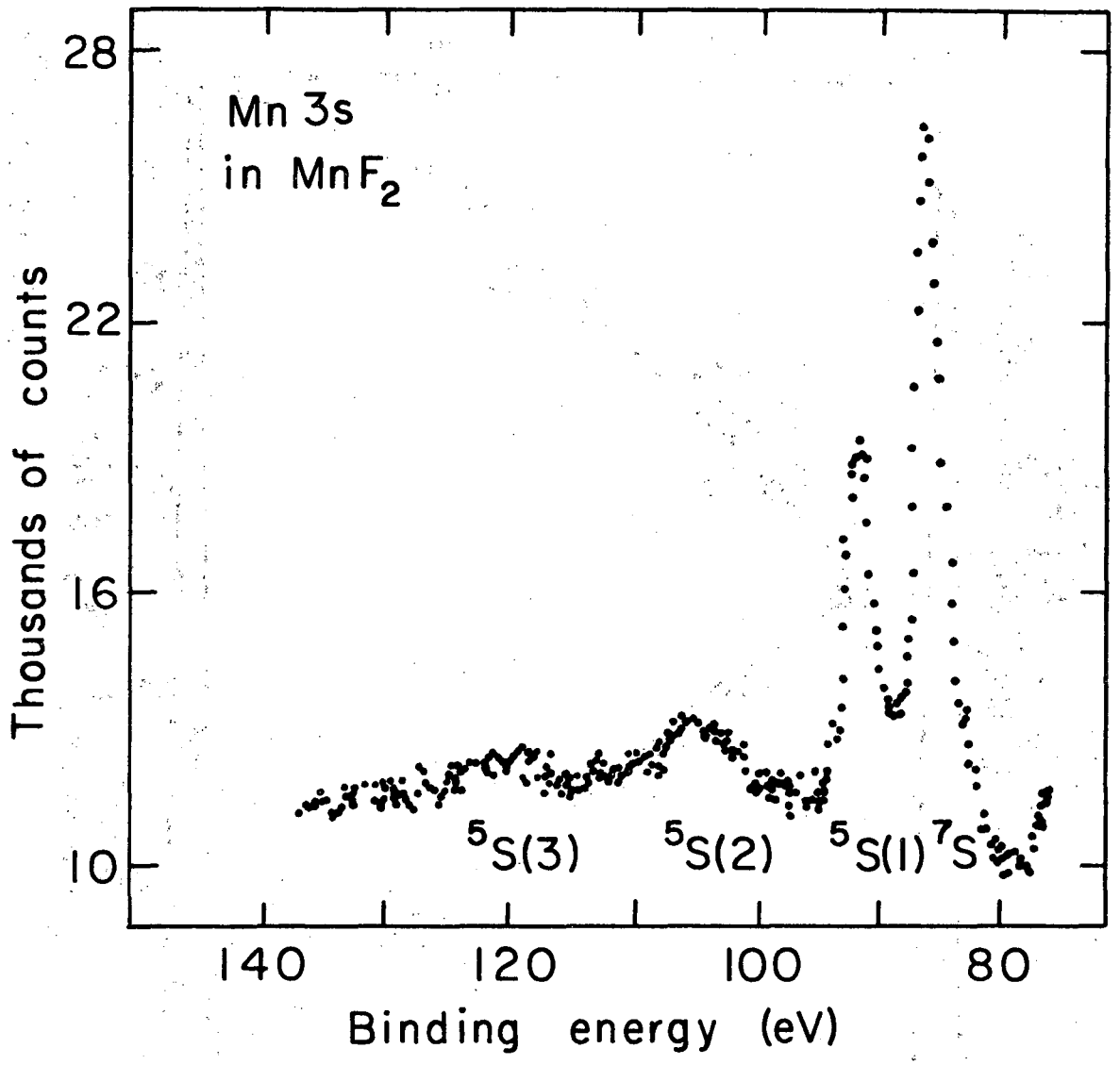

XBL745-3136

Fig. 2

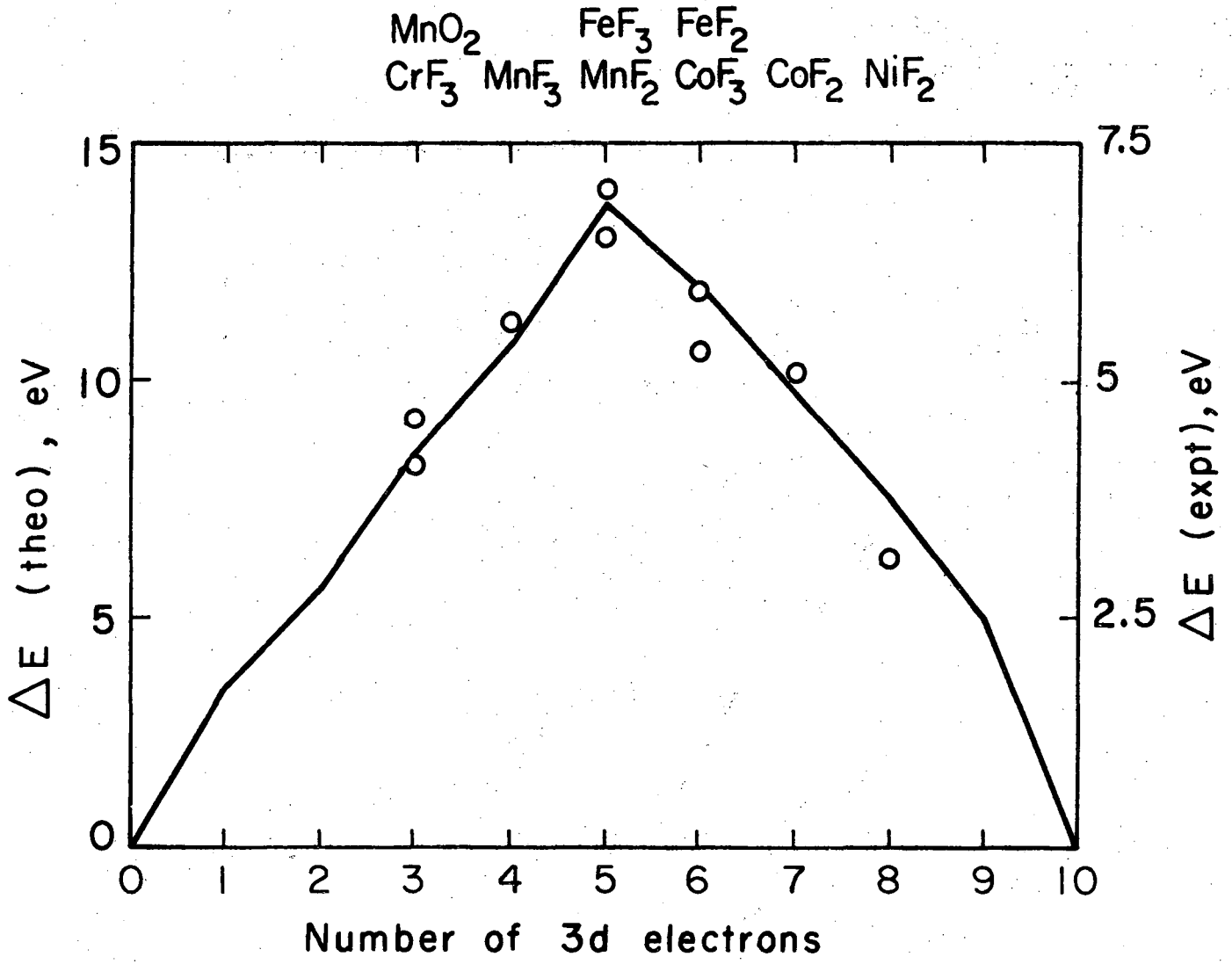

Fig. 3 XBL745-3137

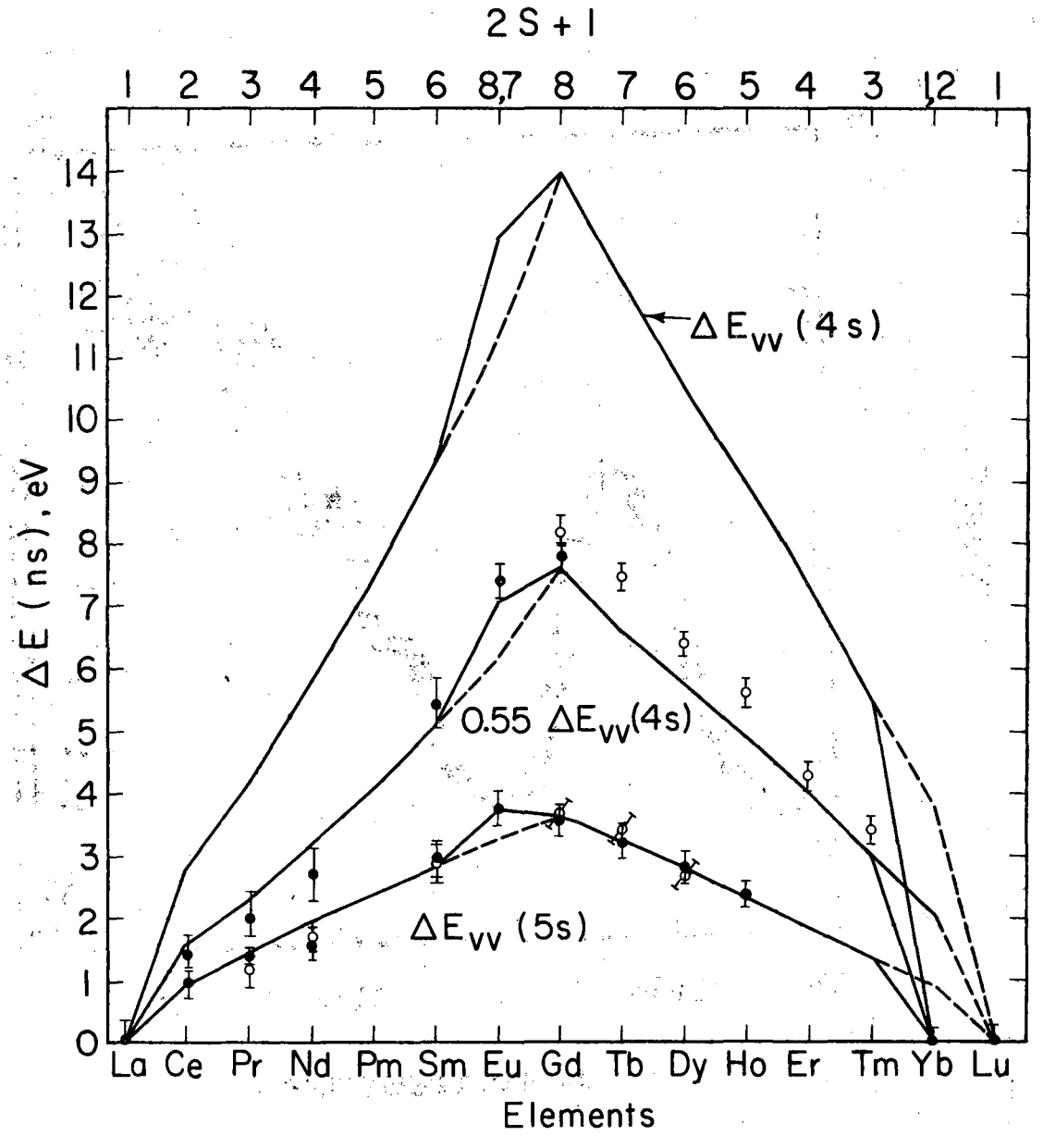

Fig. 4

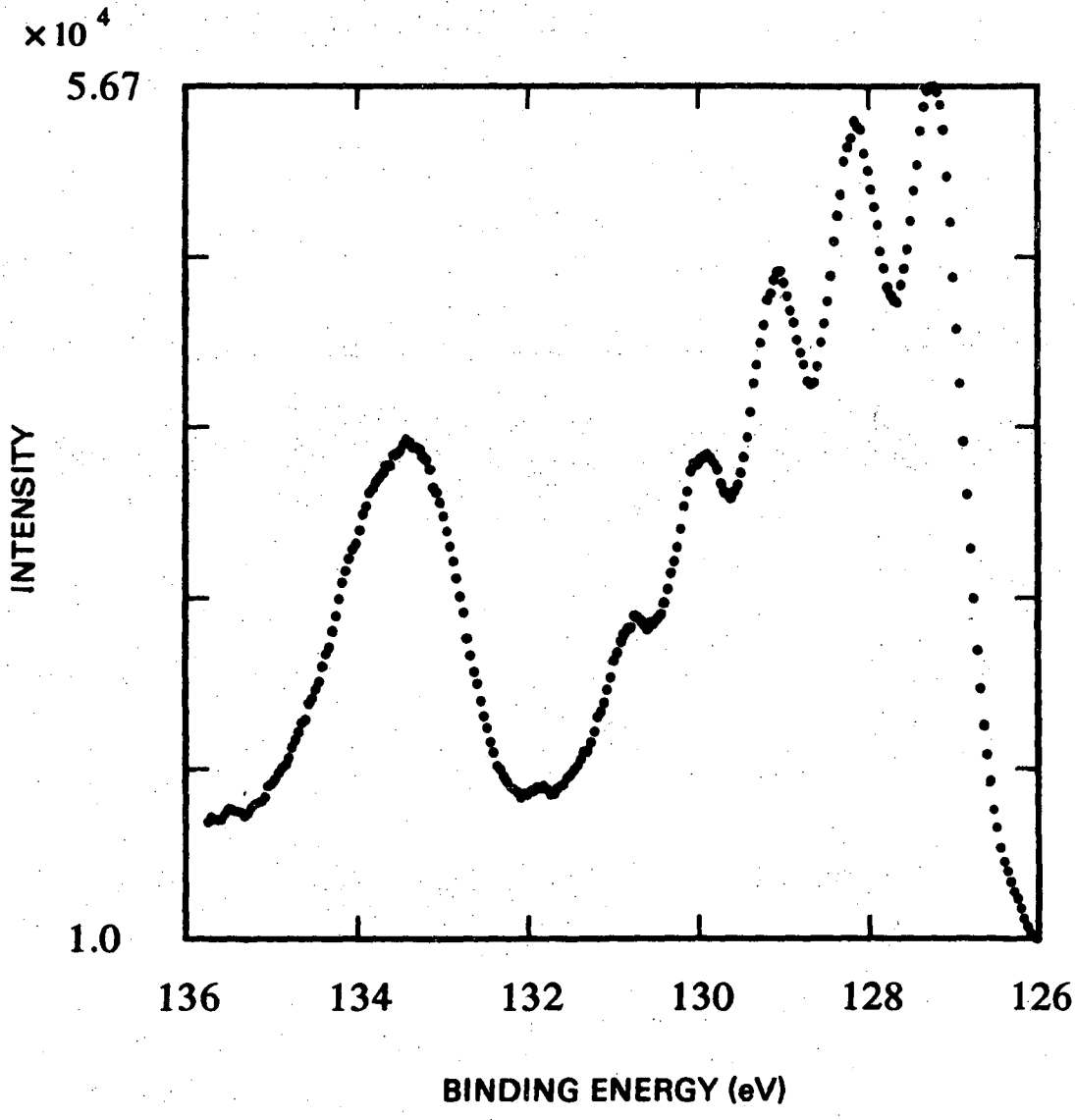

XBL 774-8516

Fig. 5

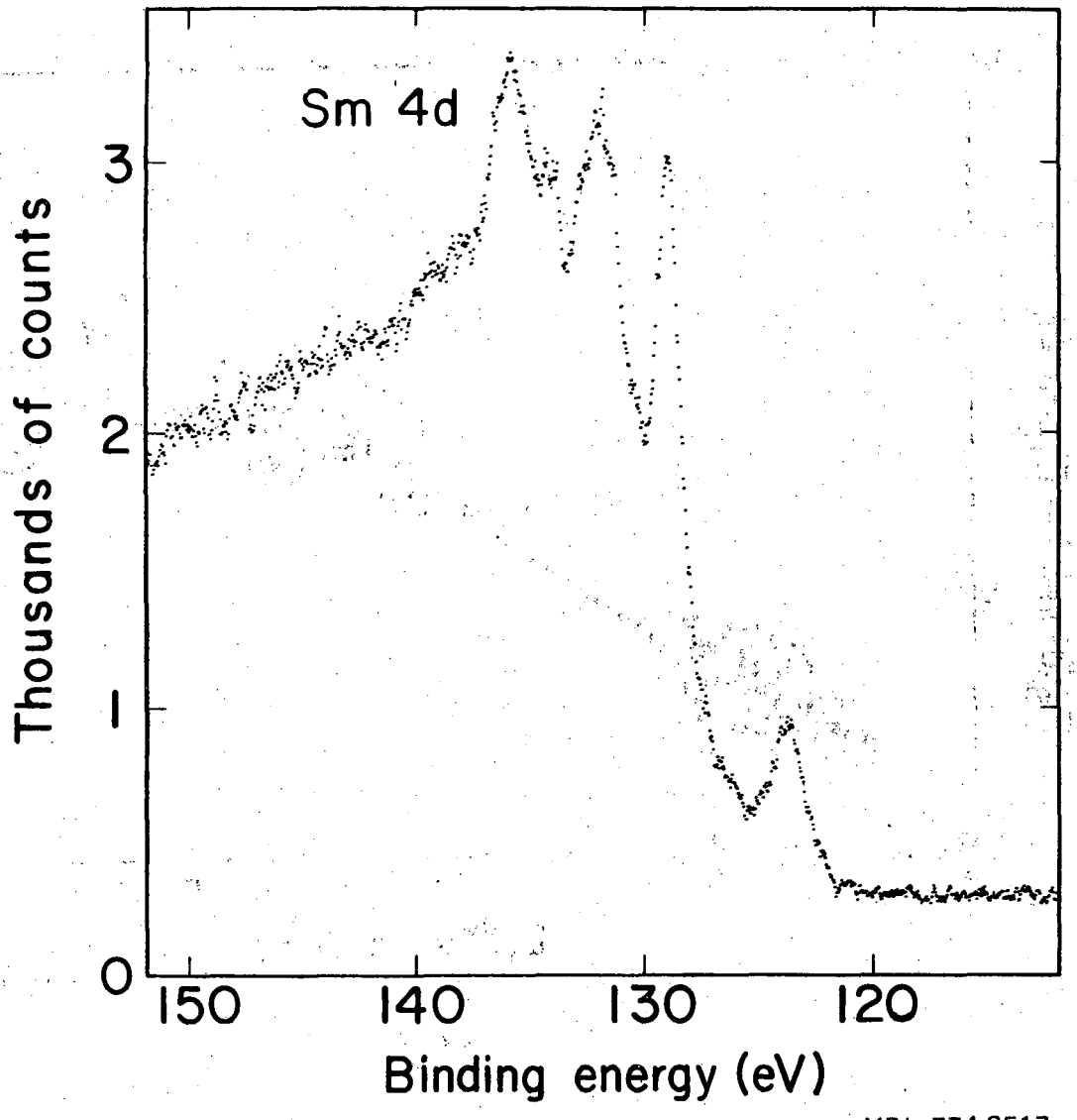

XBL 774-8517

Fig. 6

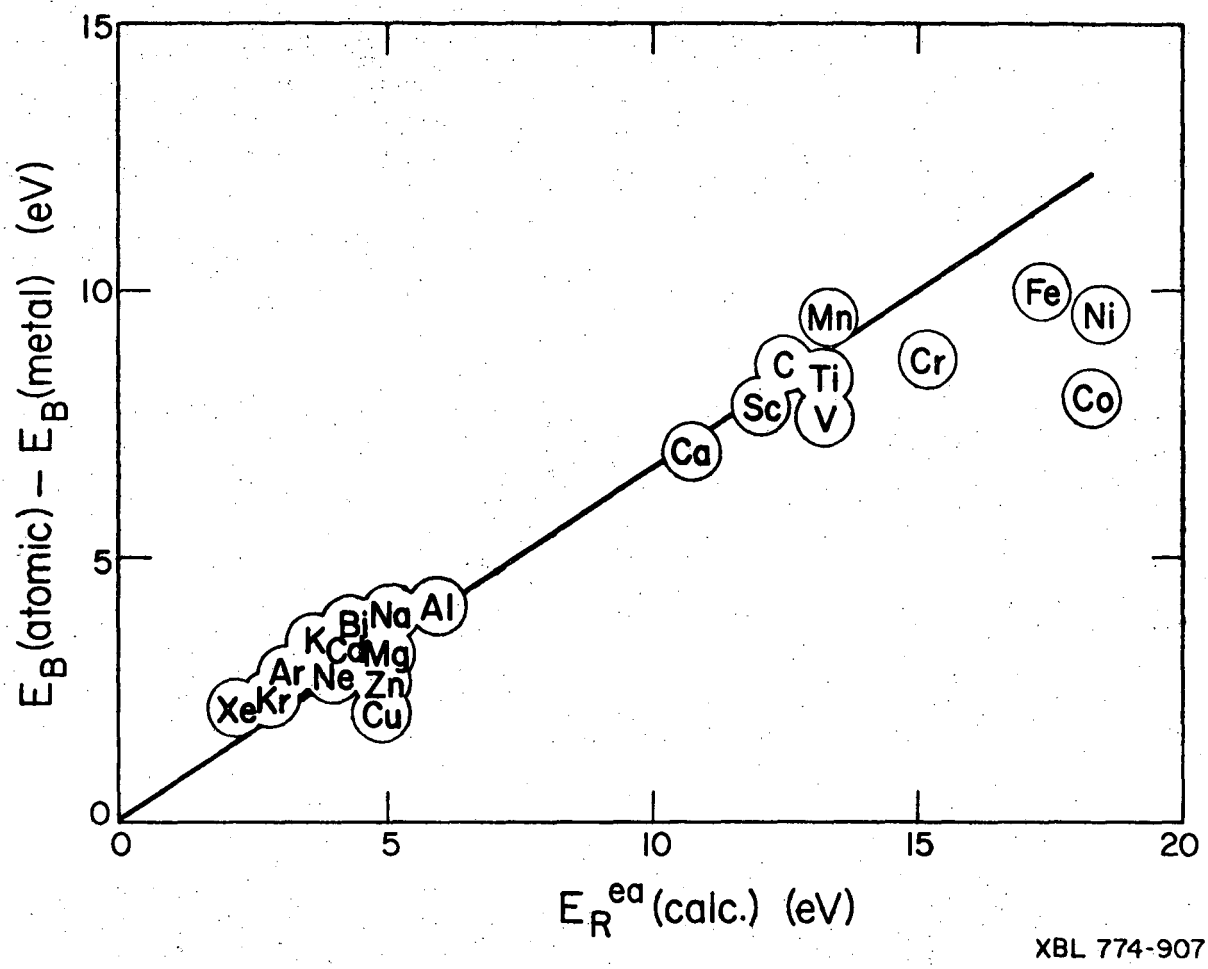
15
10
5
0
0
5
10
15
20
E_B(atomic) − E_B(metal) (eV)
E_R^{ea}(calc.) (eV)
Xe
Kr
Ar
Ne
K
Ca
Bi
Na
Mg
Al
Zn
Cu
Ca
Sc
C
Ti
V
Mn
Cr
Fe
Ni
Co
XBL 774-907

Fig. 7

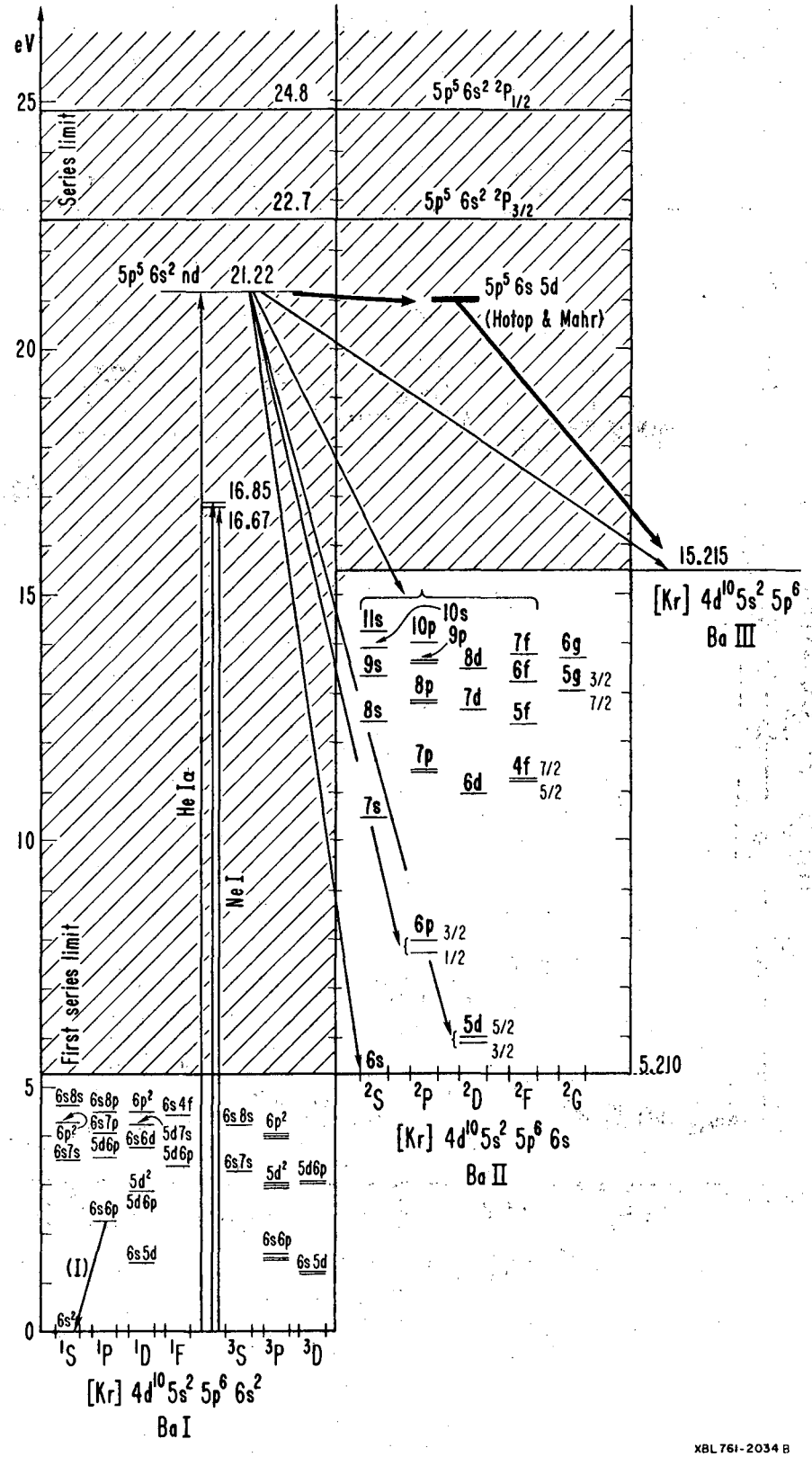
eV
25
20
15
10
5
0
24.8
$5p^5\,6s^2\,{}^2P_{1/2}$
Series limit
22.7
$5p^5\,6s^2\,{}^2P_{3/2}$
$5p^5\,6s^2\,nd$
21.22
$5p^5\,6s\,5d$
(Hotop & Mahr)
16.85
16.67
15.215
[Kr] $4d^{10}5s^2\,5p^6$
Ba III
He Ia
Ne I
First series limit
11s
10p
10s
9p
8d
7f
6g
9s
8p
6f
5g 3/2
7/2
8s
7d
5f
7p
6d
4f 7/2
5/2
7s
6p 3/2
1/2
5d 5/2
3/2
6s
5.210
^2S ^2P ^2D ^2F ^2G
[Kr] $4d^{10}5s^2\,5p^6\,6s$
Ba II
6s8s
6s8p
$6p^2$
6s4f
$6p^2$
6s7s
6s7p
6s6d
5d7s
5d6p
5d6p
$5d^2$
5d6p
6s6p
6s5d
(I)
$6s^2$
^1S ^1P ^1D ^1F ^3S ^3P ^3D
[Kr] $4d^{10}5s^2\,5p^6\,6s^2$
Ba I
XBL761-2034 B

Fig. 8

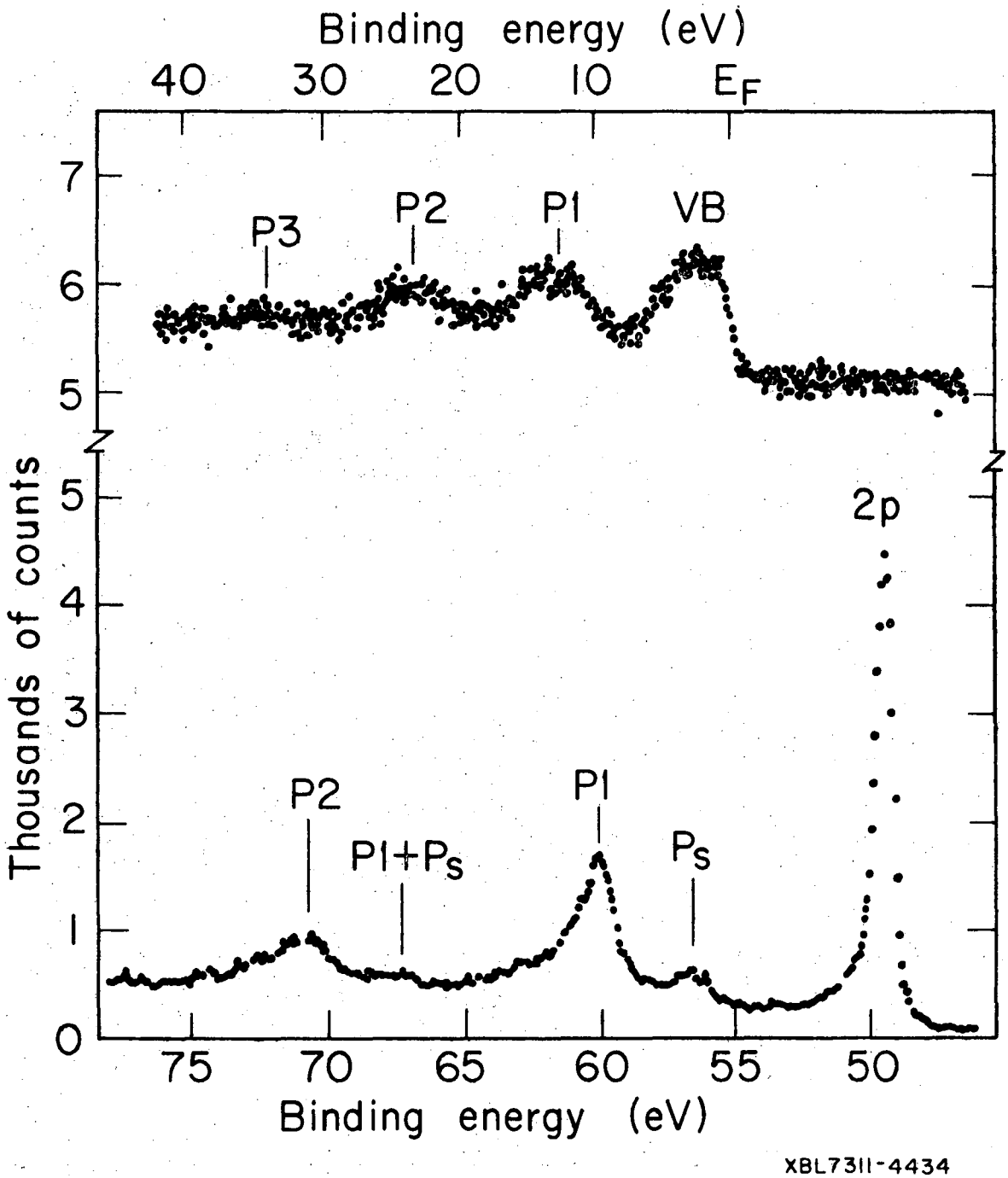
Binding energy (eV)
40
30
20
10
E_F
P3
P2
P1
VB
2p
P2
P1+Ps
P1
Ps
Thousands of counts
0
1
2
3
4
5
6
7
75
70
65
60
55
50
Binding energy (eV)
XBL7311-4434

Fig. 9

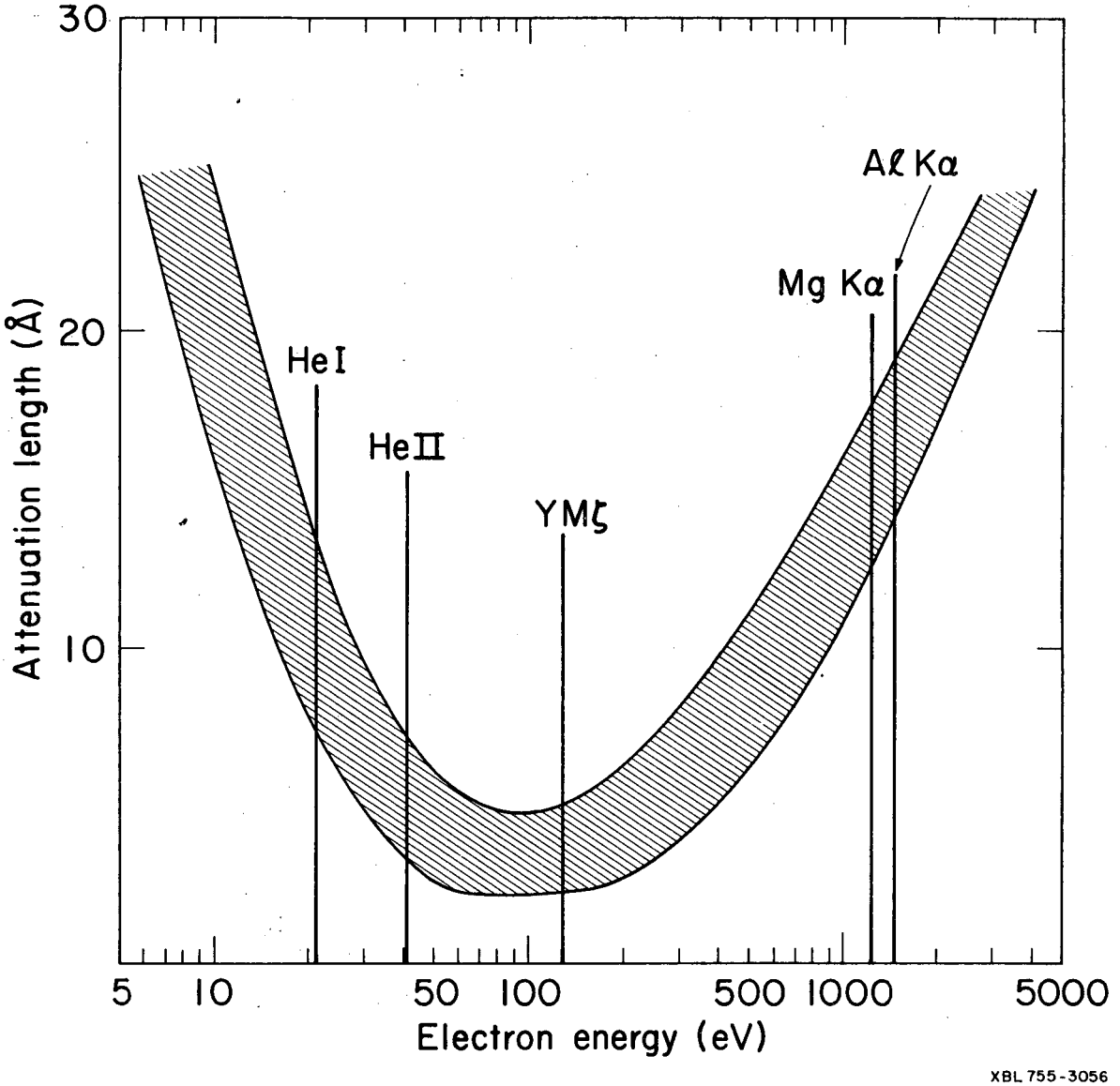

Fig. 10

This report was done with support from the United States Energy Research and Development Administration. Any conclusions or opinions expressed in this report represent solely those of the author(s) and not necessarily those of The Regents of the University of California, the Lawrence Berkeley Laboratory or the United States Energy Research and Development Administration.

TECHNICAL INFORMATION DIVISION
LAWRENCE BERKELEY LABORATORY
UNIVERSITY OF CALIFORNIA
BERKELEY, CALIFORNIA 94720